No. 039
September 1969

SYSTEMATIC RESISTANCE AND PROPULSION TESTS WITH MODELS OF SINGLE-SCREW FULL-BODIED, OIL TANKERS

Kiyoshi Tsuchida
Koichi Yokoo
Atsuo Yazaki
Shigeo Moriyama
Seizo Ohashi

THE DEPARTMENT OF NAVAL ARCHITECTURE AND MARINE ENGINEERING

THE UNIVERSITY OF MICHIGAN
COLLEGE OF ENGINEERING

Japanese Ministry of Transport
Ship Research Institute Report

Volume 1 No. 6

SYSTEMATIC RESISTANCE AND PROPULSION TESTS WITH MODELS OF SINGLE-SCREW, FULL-BODIED, OIL TANKERS.

by:

Kiyoshi Tsuchida
Koichi Yokoo
Atsuo Yazaki
Shigeo Moriyama
Seizo Ohashi

Translated by:
James L. Moss
Young T. Shen

The University of Michigan
Department of Naval Architecture and Marine Engineering
Ship Hydrodynamics Laboratory

September, 1969

Translators' Note

This paper contains much useful information for estimating still water resistance and propulsion performance of full hull forms with single screw propulsion, specifically large bulk carriers.

The naval architect finds that for purposes of performance prediction of full hull forms systematic series data is largely non-existent. The more commonly used series, such as Series 60, Taylor Standard Series and the BSRA Series, are often not applicable since the type of hull form may be inappropriate, the range of major ship proportions covered may not encompass proportions of interest or the basic fullness of series hull forms may not be great enough. Usually information on hull forms with low length-beam ratio and with block coefficient greater than 0.80 is scarce.

The series reported on in this paper tends to fill the void in the existing literature. Block coefficients as high as 0.84 and L/B nearly as low as 6.00 are covered. Moreover, data on both resistance and propulsion in two ballasted or lightly laden conditions are included. To the translators knowledge, no systematic series data in other than fully laden conditions otherwise exists. Therefore, this paper is considered to be of special importance to design of bulk carriers and its availability in the English language is most desirable.

The permission of the authors to publish this translation and to directly reproduce their figures is gratefully acknowledged.

J.L. Moss
Y.T. Shen

Ann Arbor
September, 1969

NOMENCLATURE

a:	Wetted surface area coefficient
B:	Breadth, m
C_B:	Block coefficient
d:	Draft, m
F_n:	Froude number
g:	Acceleration of gravity, m/sec^2
l_{CB}:	Location of the center of buoyancy, %Lpp from ⊠, -fwd, +aft
L, L_{pp}:	Length between perpendiculars, m
L_{DWL}:	Design water line length for full load conditions, m
r_F:	Frictional resistance coefficient
r_R:	Residuary resistance coefficient
R:	Total resistance, kg
R_F:	Frictional resistance, kg
R_R:	Residuary resistance, kg
R_n:	Reynolds number
S:	Total wetted surface area, m^2
S':	Wetted surface area, without bilge keels, m^2
t:	Thrust deduction fraction
v:	Speed, m/sec
w_m:	Model ship wake fraction
w_s:	Actual ship wake fraction

NOMENCLATURE [cont.]

w_Q: Wake fraction based on torque identity method

w_T: Wake fraction based on thrust identity method

η: Propulsive efficiency

η_o: Propeller efficiency (open water)

η_R: Relative rotative efficiency

∇: Volumetric displacement, m^3

CONTENTS

I. Introduction

About ten years ago, in the Ship Research Institute Propulsion Branch (previously the Transportation Research Institute Ship Propulsion Branch), several series of systematic model tests were conducted on large tankers. Recently, because the size of tankers has been increasing in tonnage and length, it was decided to continue those tests and to include all test results up to the present. This report contains information from all the model tests that will be of value in the basic planning of the super-tankers of the future.

II. Model Ships

Thirty-five models of different block coefficients and of different proportions, as shown in Table 1, were tested. All model lengths were 6.00 meters between perpendiculars. Models 1188, 1189, 1190, 1321, 1322, 1323, 1324, and 1325 were made of wood and the rest were made of paraffin wax.

The model tests were divided into several series, as indicated in Table 1. Since most of the tests were made for shipyards, it was necessary to choose the following characteristics in uniform order to compare hulls from different parent forms.

1. C_B Series

Aside from the rate of change in C_B, the shape of the sectional area curve was kept the same as that of the parent. The auxiliary body line shape in each transverse section was made so that the body plan, $b/b' = \frac{1-P}{1-P'}$. (The symbols are explained in the figures.) However, around the stem and stern some refairing was necessary.

2. L/B Series

The shape of each transverse section was considered to be similar to the others. Therefore, actual dimensions were changed according to the value of L/B.

3. B/d Series

According to the increases or decreases in draft, the shapes of the cross sections were expanded or compressed in the direction of the draft. However, this resulted in bilges of elliptical shape, which was considered impractical. The bilge shapes were therefore replaced by circular arcs approximately equivalent to the previously obtained ellipse.

The ranges of C_B, L/B, B/d for the models are shown in Figure 1. Taking M.S. 1321 as an example, the following figures are presented:

As shown by Figure 2, the stems were representative of ships without large bulbous bows.

III. Model Propeller

The propeller used was M.P. 487. Its shape and main dimensions are shown in Figure 5, and its open water characteristic curves are shown in Figure 6. The propeller position in the stern aperture is shown in Figure 4.

IV. Test Conditions

Three different loading conditions were used in the towing tank tests.

1. Full load condition (even keel)
2. Half load condition (65% of the full load displacement, 1% L_{pp} stern trim)
3. Ballast condition (44% of the full load displacement, 2% L_{pp} stern trim).

The resistance and self-propulsion tests for the models were always conducted with all apendages except bilge keels. Turbulent flow was stimulated by trapezoidal studs 1 mm high, spaced 1 mm apart and located in a single row at station 9 1/2.

For frictional resistance calculations Schoenherr's equation was used. The correction of frictional resistance in self-propulsion tests was based on length between perpendiculars. No correlation allowance was made.

V. Analysis

1. Resistance

From the resistance test results, the calculated value of residuary resistance coefficient, using the following equation, was plotted in the shape of contour curves with L/B on the abscissa and C_B on the ordinate:

$$r_R = {}^{R_R}/_{\rho \nabla^{2/3} v^2} \qquad (1)$$

where $R_R = R - R_F$

∇ = Displacement (m^3)

v = Speed (m/sec)

ρ = Fluid density (kg sec^2/m^4)

R = Total resistance of model ship (kg)

R_F = Calculated model frictional resistance based on Schoenherr's equation (kg).

The results shown in Figures 7 through 50, the contents of which are as follows:

Figure Number	Load Condition	B/d	$F_n = v/\sqrt{g\, L_{DWL}}$
7-14	Full Load	2.46	0.14,0.16,0.17,0.18,
15-22		2.76	0.19,0.20,0.21,0.22
23-29	Half Load	2.46	0.14,0.16,0.18,0.19,
30-36		2.76	0.20,0.21,0.22
37-43	Ballast	2.46	0.14,0.16,0.18,0.19,
44-50		2.76	0.20,0.21,0.22

In order to show the effect of C_B and L/B on r_R, Figures 51 through 56 are given. In Figures 51 through 54, for different values of C_B, the residuary resistance coefficient, r_R, for the

full load condition, is shown with L/B as abscissa and F_n and B/d as parameters. Figures 55 and 56 show the full load condition residuary resistance coefficient, r_R, versus F_n for values of L/B in the case of B/d = 2.76 with C_B as the parameter.

2. Self-Propulsion Factors

From the test results, $1-w_T$, $1-t$, η_R and $\frac{1-t}{1-w_T}\eta_R$ were obtained. Their variations, with respect to C_B and L/B are shown in Figures 57 and 59. During the process of making those figures, the possible effect of B/d was also investigated. Inside the B/d range for this series test, no systematic variation with respect to B/d was observed.

In Figures 60 to 65, the factors mentioned previously are shown in contour curves with L/B as abscissa and C_B as ordinate. However, the self-propulsion factors given here were based on the Froude number of 0.16. If application is made using Figures 60 to 65, the following considerations should be taken into account:

a. The correction when the Froude number is not 0.16

According to the test results, $1-t$ and η_R could be considered as constants with respect to Froude number within the 0.14 to 0.22 range of Froude numbers. However, $1-w_T$ has considerable variation.

The variation of $1-w_T$ with respect to Froude number between values of 0.16 and 0.20 can be given approximately by the equations:

Full load condition:

$$(1-w_T)_{0.20} = (1-w_T)_{0.16} / 0.980 \quad (2)$$

Half load condition:

$$(1-w_T)_{0.20} = (1-w_T)_{0.16} / 0.955 \quad (3)$$

Ballast condition:

$$(1-w_T)_{0.20} = (1-w_T)_{0.16} / 0.940 \quad (4)$$

The value of $\frac{1-t}{1-w_T}\eta_R$ also varies with respect to Froude number; however, this is due to the variation of $1-w_T$ as mentioned previously.

b. The value of $1-w_T$ was obtained by the thrust identity method, so if the wake coefficient, w_Q, based on the torque identity method, is desired, a conversion is required. This conversion can be expressed approximately as:

$$(1-w_Q) = (1-w_T)\left(1+\frac{\eta_R - 1}{0.70}\right) \quad (5)$$

c. All the values given in Figures 60 to 65 were based on the model data, and possible scale effects must therefore be considered. The self-propulsion factors $1-t$ and η_R

can be used in practical applications without significant error. However, in the cases of $1-w_T$ or $1-w_Q$, scale effects cannot be ignored.

d. The values of self-propulsion factors, as stated previously, were based on the use of a four-bladed propeller in the self-propulsion tests. If the ratio of propeller diameter to ship dimensions was remarkably different from our case (as shown in Figure 5), the values of 1-w were corrected.

VI. Application of Resistance and Self-Propulsion Factors

By using the figures, the resistance and self-propulsion factors for a super-large ship can be investigated. Also, the effective horsepower and delivered horsepower can be estimated. For example, first, using Figures 7 to 50, and using the appropriate values of C_B, L/B, and B/d, the residuary resistance coefficient, C_R, for a given ship hull can be read for each Froude number. If the value of B/d is between 2.46 and 2.76, a linear interpolation can be used.

Next, the frictional resistance coefficient, C_F, for each Froude number can be obtained according to Schoenherr's equation. To this is added a suitable correlation allowance coefficient, C_A.

Using the following equations, residuary resistance, R_R, and frictional resistance, R_F, are calculated for each Froude number.

$$R_R = r_R \cdot \rho \nabla^{2/3} v^2 \tag{6}$$

$$R_F = (C_F + C_A) 1/2 \rho S v^2 \tag{7}$$

Where ∇ is the actual ship displacement (m^3), v the ship speed corresponding to the correct Froude number (m/s), S the actual

ship wetted surface area including bilge keels (m^2), C_F is the calculated ship frictional resistance coefficient based on Schoenherr's equation with the Reynolds number corresponding to the Froude number, C_A is the correlation allowance coefficient, and ρ is the fluid density.

The value of wetted surface area, without bilge keels, in case it is unknown, can be approximated as follows:

$$S' = aLd + \frac{\nabla}{d} \tag{8}$$

where L is the length between perpendiculars (m), d is the average draft (m), ∇ is the displacement (m^3), and a is a constant. In the full load condition, a is 1.81; in the half load condition, 1.76; and in the ballast condition, 1.75.

The total resistance, R, is obtained from R_R and R_F, and the effective horsepower, P_E, corresponding to the appropriate Froude number can be expressed as:

$$P_E = \frac{Rv}{75} \tag{9}$$

Next, using the ship's C_B, L/B, B/d, etc., and Figures 60 to 65, the self-propulsion factors of the model ship can be obtained. Of the self-propulsion factors, the value of $1-w_T$ can be corrected to the actual ship's value since the value is affected significantly by scale effects. During this process, if $1-w_Q$ is used instead of $1-w_T$, equation (5) can be applied. Moreover, if the ratio of the propeller diameter to the ship's

dimensions is different from that is this systematic series, an additional correction of 1-w must be made. The constant propeller efficiency η_o is obtained from the figure and table relating to the propeller.

Finally, the propulsive coefficient can be computed from

$$P_D = \frac{P_E}{\eta} \tag{10}$$

From the computations demonstrated, it is possible to obtain the effective horsepower curves and delivered horsepower curves for various Froude numbers and loading conditions.

The computations just outlined can be applied to compute, with good accuracy, the horsepower for a super-large ship if the ship has a similar form, as shown in Table 1 and Figure 1. If the ship form is quite different, the accuracy of the calculations will be reduced.

VII. Numerical Example

The horsepower of a tanker is calculated by the method stated in Section VI and is compared with the towing tank results.

The procedure used to compute the horsepower is shown in Table 3, and the comparison with the towing tank test is shown in Figure 66.

For this numerical example, the tanker is:

Ship body: General stem and stern shape

L_{DWL} = 221.60 m l_{CB} = -1.50%

L_{pp} = 217.00 m B = 31.00 m

d = 11.49 m C_B = 0.796

Main machinery: 18,000 shp x 110 rpm

Propeller = single-screw, 5-blade AU type

D = 6.60 m

H/D = 0.764

A_E = 0.610

C_A = 0.0002 (Schoenherr's equation).

$$\frac{1-w_s}{1-w_m} = 1.20$$

From Figure 66, according to the results computed by this method, the propulsive properties can be estimated with good accuracy.

VIII. Acknowledgments

Thanks are due to Japan Jouson Institute, Nichelizu Shipyards, Incorporated, Michuldo Shipyards, Incorporated, and Kawazuki Heavy Industry, Incorporated for supporting this series test.

Thanks are also due to each staff in Michuido Shipyards, Incorporated and Kawazuki Heavy Industry, Incorporated for their help in analyzing the test results.

IX. References

1. Atsuo Yazaki *et al*, "The Relationship in Wake Fraction Obtained from the Thrust Identity Method and Torque Identity Method," The Transportation Research Reports 43 and 58.

2. Koichi Yokoo, "An Investigation into Ship Model Correlation," Transportation Institute Report (in English) 45.

3. T.P. O'Brien, "The Design of Marine Screw Propellers," 1962, p. 143.

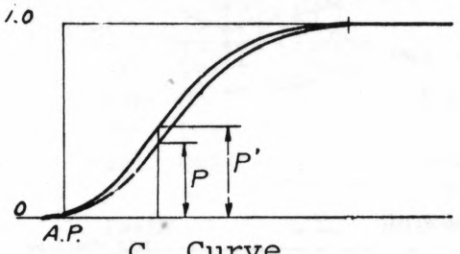

C_P Curve

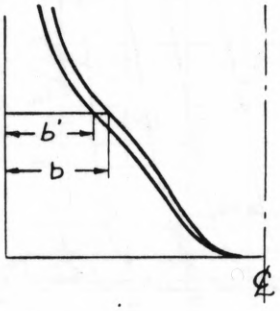

Body Plan

M.S. No.	C_B	L/B	B/d
987	0.78	7.34	2.46
988	0.80	〃	〃
989	0.82	〃	〃
990	0.84	〃	〃
1125	0.78	6.983	2.59
1126	0.80	7.163	2.525
1127	0.84	7.519	2.406
1188	0.80	7.00	2.46
1189	〃	7.20	〃
1190	〃	7.60	〃
1321	〃	7.34	〃
1322	0.82	7.00	2.46
1323	〃	7.20	〃
1324	〃	7.34	〃
1325	〃	7.60	〃
1152	0.80	7.839	2.16
1153	〃	6.935	2.76
1154	0.82	7.839	2.16
1155	〃	6.935	2.76
1506	0.80	6.75	2.76
1507	0.82	〃	〃
1508	0.80	6.50	〃
1509	0.82	〃	〃
1548	0.84	6.50	〃
1549	0.84	6.25	〃
1550	0.82	〃	〃
1564	0.82	6.75	2.46
1565	0.80	〃	〃
1566	0.82	6.17	3.06
1567	0.80	〃	〃
1551	0.84	6.50	2.46
1552	0.82	6.25	〃
1553	0.80	〃	〃
1554	0.78	6.50	〃
1555	0.80	6.25	2.76

Table 1

Fig.1 Pattern of Geometorical Variation of Model Proportions

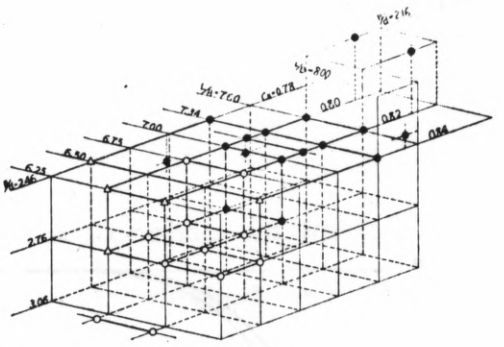

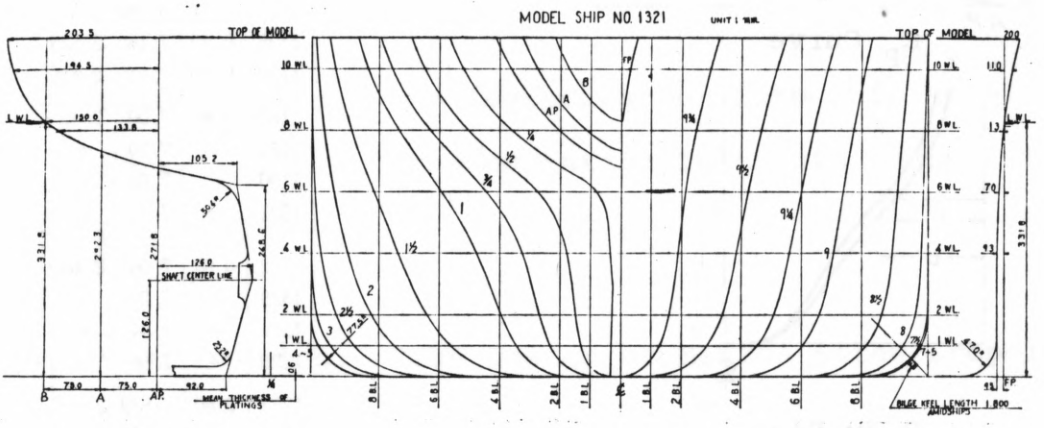

Fig.2 Body Plan, Stem & Stern Contour [M.S. No. 1321]

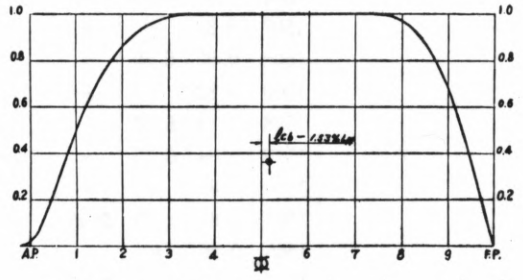

Prismatic Curve

Fig.3 Prismatic Curve of M.S. No. 1321

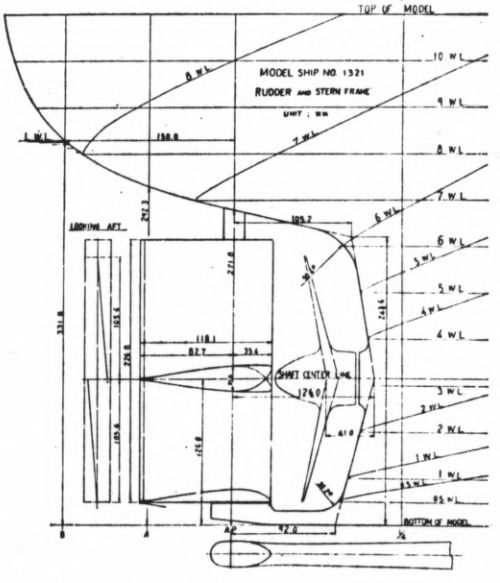

Fig.4 Stern Frame & Rudder of M.S. No. 1321

Table 2
M.S. No.1321

L_{PP} (m)	6.000
L_{DWL} (m)	6.150
B (m)	0.8172
d (m)	0.3318
∇ (m^3)	1.3017
L_{PP}/B	7.342
B/d	2.463
$\nabla/(L_{PP}^3\times 10)$	6.027
C_B	0.800
C_P	0.808
C_M	0.990
l_{CB} (%)	−1.53

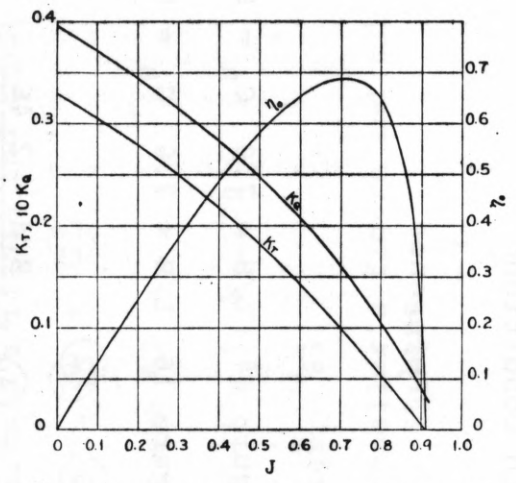

Fig.6 Characteristic Curve of M.P. No. 487

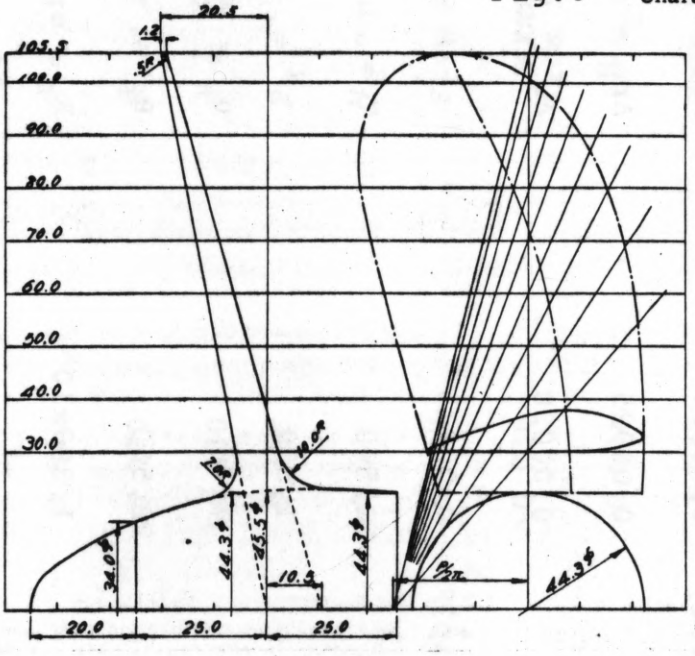

Fig.5 M.P. No. 487

DIAMETER	211.0
BOSS RATIO	.210
PITCH	162.4
PITCH RATIO	.770
EXPANDED AREA RATIO	.405
MAX. BLADE WIDTH RATIO	.229
BLADE THICKNESS RATIO	.050
ANGLE OF RAKE	11°~0°
NUMBER OF BLADES	4
DIRECTION OF TURNING	RIGHT HANDED

Unit in mm

TABLE 3

Froude Number 0.16 at Full Loaded Condition

No.	Coefficient	Value	Reference
①	F_n	0.16	
②	r_R (B/d = 2.46)	0.00295	From Figure 8 L/B = 7.0 C_B = 0.796
③	r_R (B/d = 2.76)	0.00320	From Figure 16 L/B = 7.0 C_B = 0.796
④	Δr_R	0.00025	Δr_R = ③ - ②
⑤	$\Delta r_{R\ corr}$	0.00020	$\Delta r_{R\ corr}$ = ④ x $\frac{B/d - 2.46}{0.3}$, B/d = 2.70
⑥	r_R (this ship)	0.00315	
⑦	$\nabla (m^3)$	61,540	∇ = L x B x d x C_B
⑧	$\nabla^{2/3}$	1,559	
⑨	v_s (m/sec)	7.46	$v_s = F_n \sqrt{L_{DWL} g}$, $\sqrt{g}$ = 3.1305
⑩	R_R (kg)	28,560	$R_R = \rho \nabla^{2/3} v_s^2 r_R$, ρ = 104.51 kg sec^2/m^4
⑪	R_n	1.393×10^9	$R_n = L_{DWL}\ v_s/\nu$, $\nu = 1.187 \times 10^{-6}$ (15°C)
⑫	C_F	1.470×10^{-3}	Schoenherr's frictional resistance coefficient
⑬	C_A	-0.2×10^{-3}	

TABLE 3 (cont.)

(14)	C_{FS}	1.270×10^{-3}	C_{FS} = (12) + (13)
(15)	S(m^2)	9,847	$S = aLd + \frac{\nabla}{d}$, without bilge keel
(16)	R_F(kg)	36,370	$R_F = 1/2\rho S v_s^2 C_{FS}$
(17)	R (kg)	64,930	R = (10) + (16)
(18)	P_E	6,458	$P_E = Rv_s/75$ = (17) x (9)/75
(19)	V_s (knots)	14.5	$V_s = 1.944 v_s$ = 1.944 x (9)
(20)	$1-w_T$	0.574	From Figure 60
(21)	$\Delta(1-w_T)$	-0.036	Correction with respect to propeller diameter from Harvald's figure and table
(22)	$(1-w_T)$	0.538	$(1-w_T)_1$ = (20) + (21)
(23)	η_R	1.032	From Figure 63
(24)	$1-w_{TS}$	0.646	$1-w_{TS} = (1-w_T)_1 \times 1.20$
(25)	1-t	0.792	From Figure 63
(26)	η_o	0.565	From propeller's figure and table estimated with thrust base

TABLE 3 (cont.)

(27)	η	0.714	η = (23) (25) (26) / (24)
(28)	P_D	9,045	P_D = (18) / (27)
(29)	P_S	9,225	P_S = 1.02 (28)

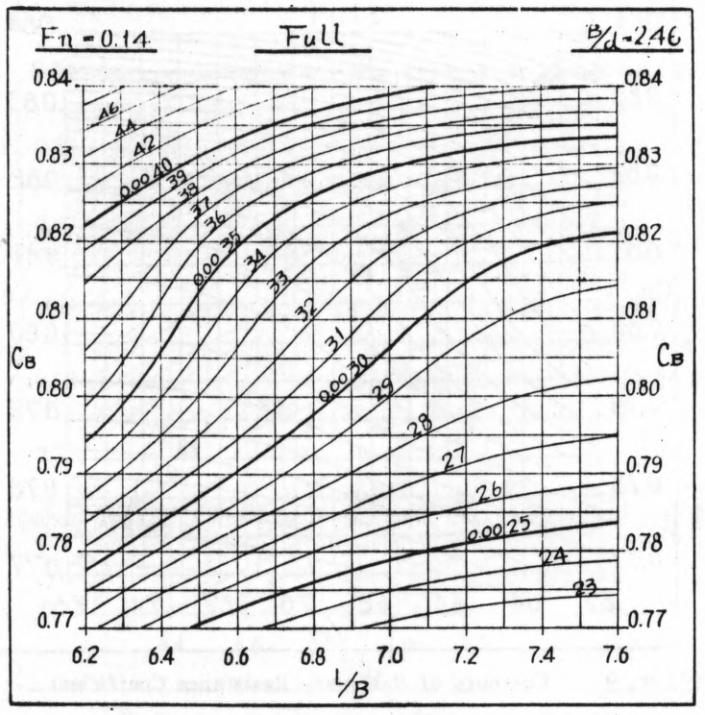

Fig.7 Contours of Residuary Resistance Coefficient

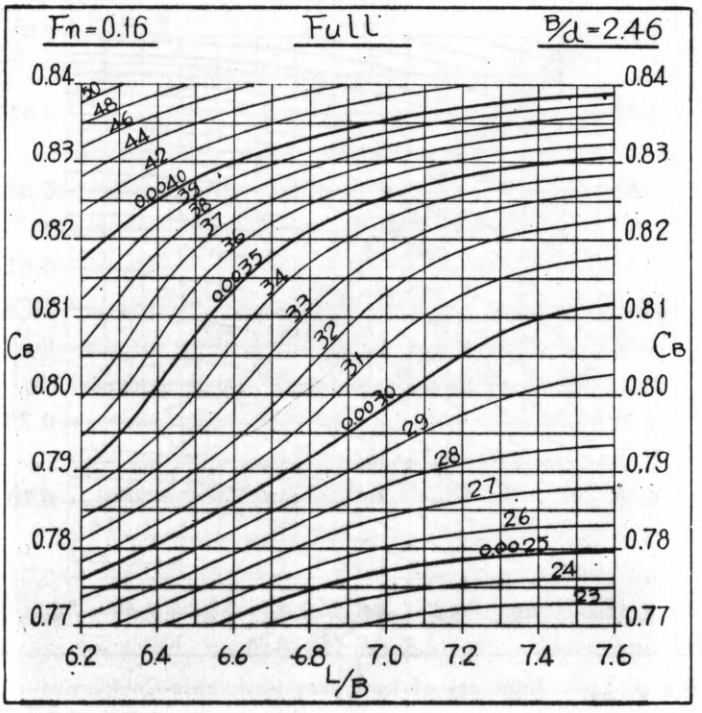

Fig.8 Contours of Residuary Resistance Coefficient

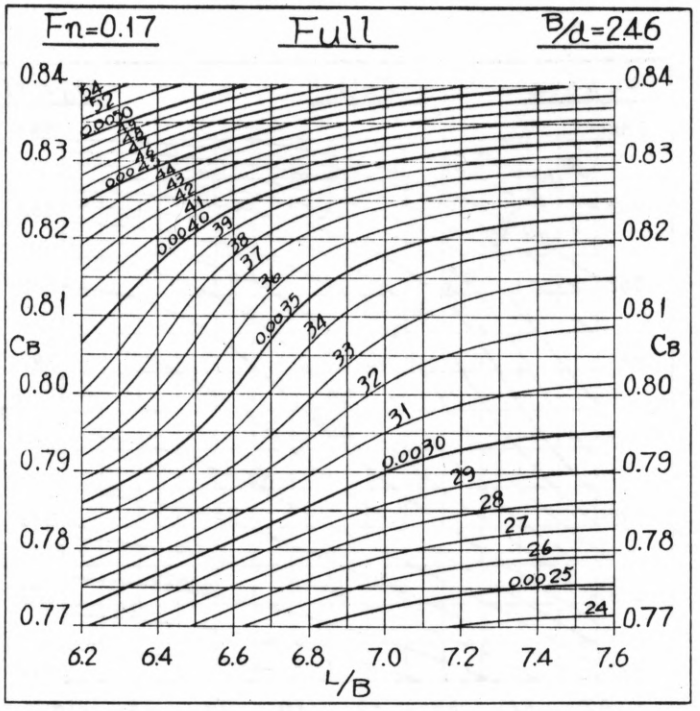

Fig.9 Contours of Residuary Resistance Coefficient

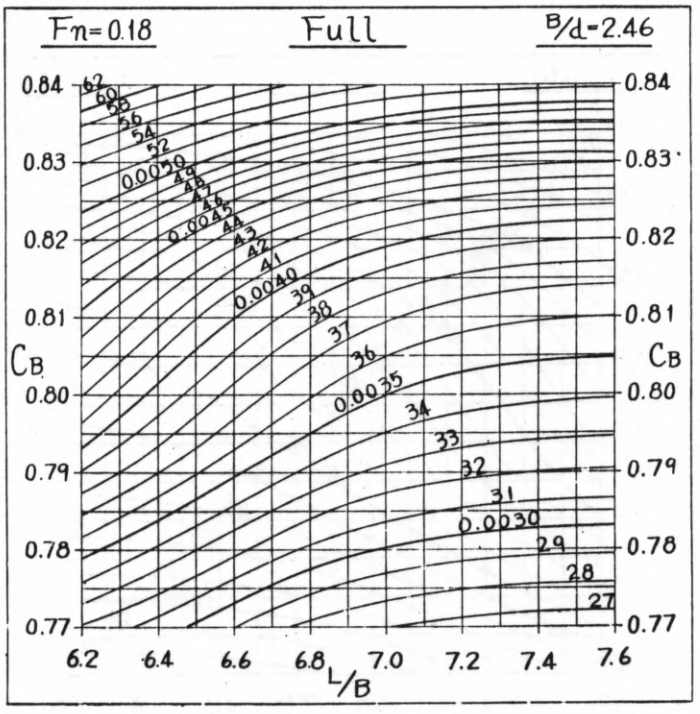

Fig.10 Contours of Residuary Resistance Coefficient

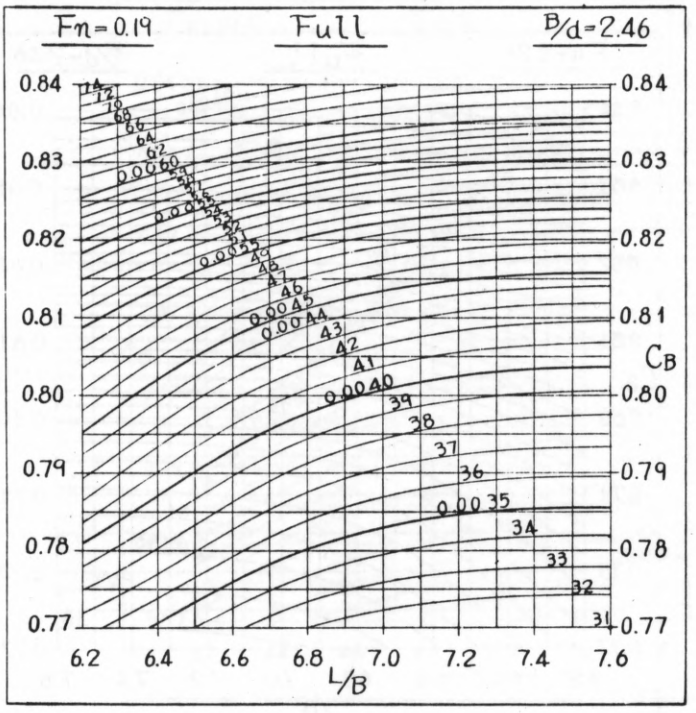

Fig.11 Contours of Residuary Resistance Coefficient

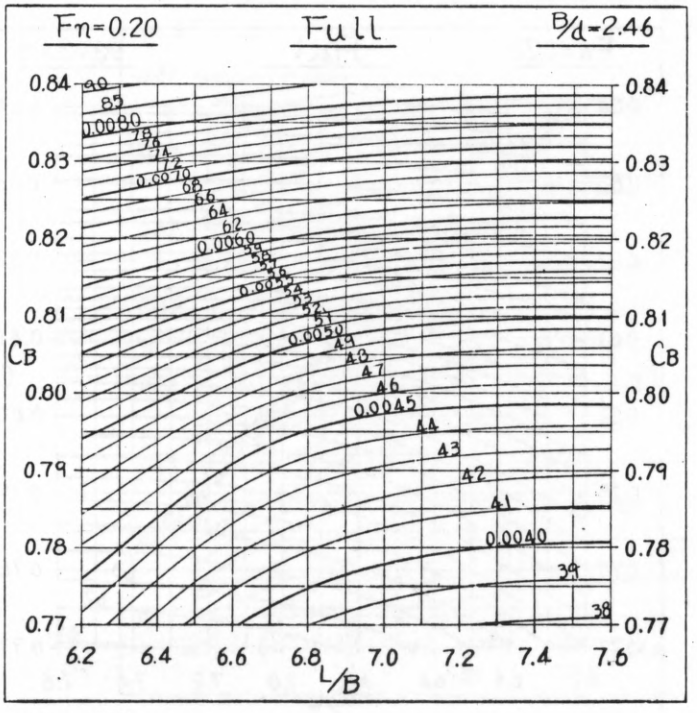

Fig.12 Contours of Residuary Resistance Coefficient

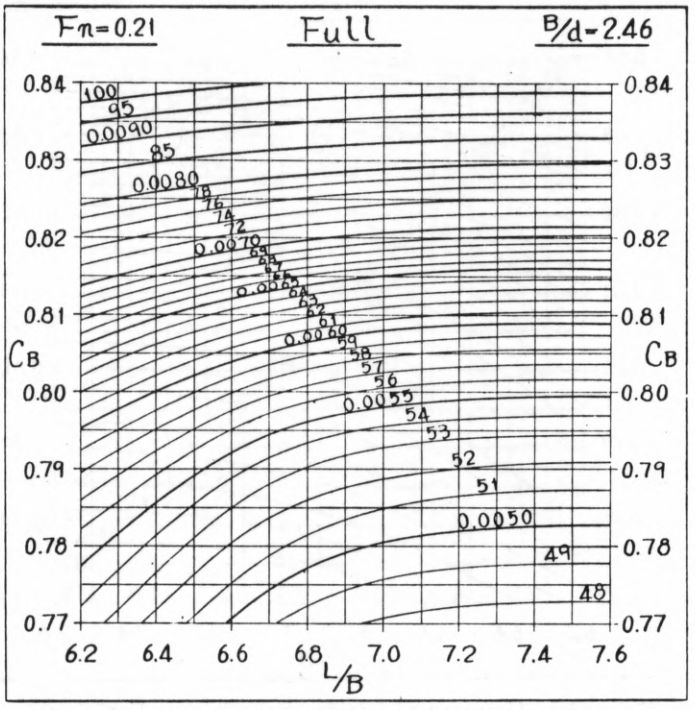

Fig.13 Contours of Residuary Resistance Coefficient

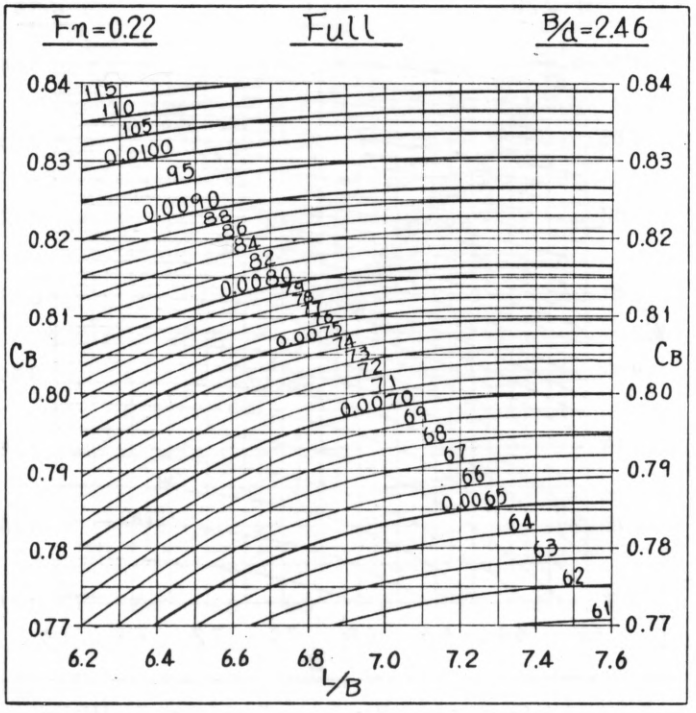

Fig.14 Contours of Residuary Resistance Coefficient

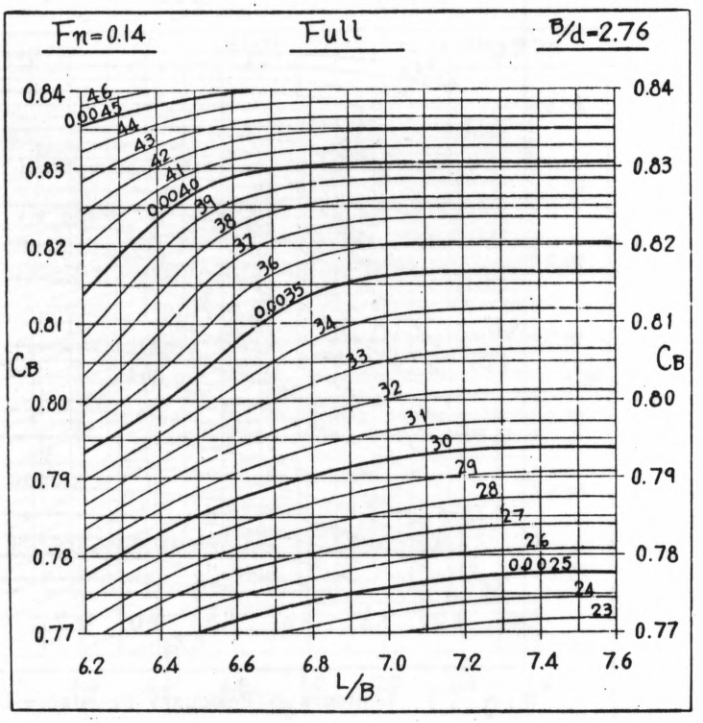

Fig.15 Contours of Residuary Resistance Coefficient

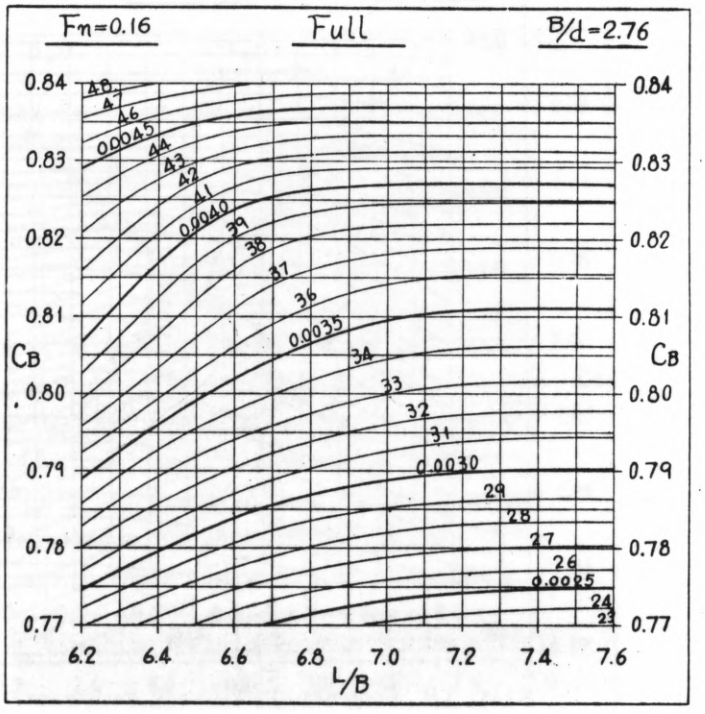

Fig.16 Contours of Residuary Resistance Coefficient

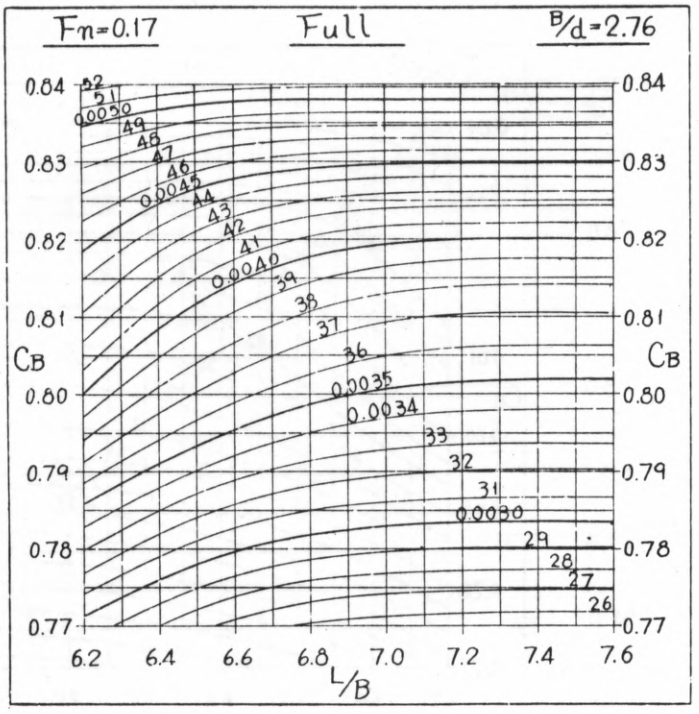

Fig.17 Contours of Residuary Resistance Coefficient

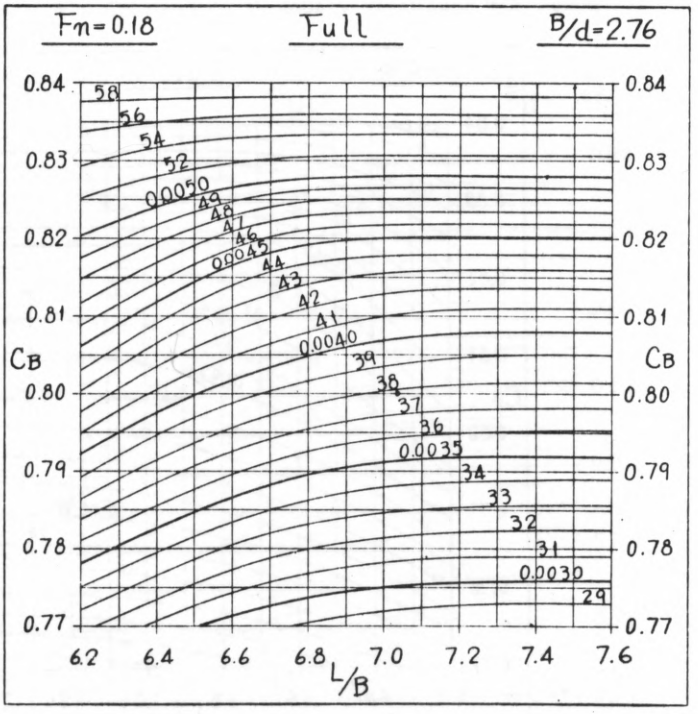

Fig.18 Contours of Residuary Resistance Coefficient

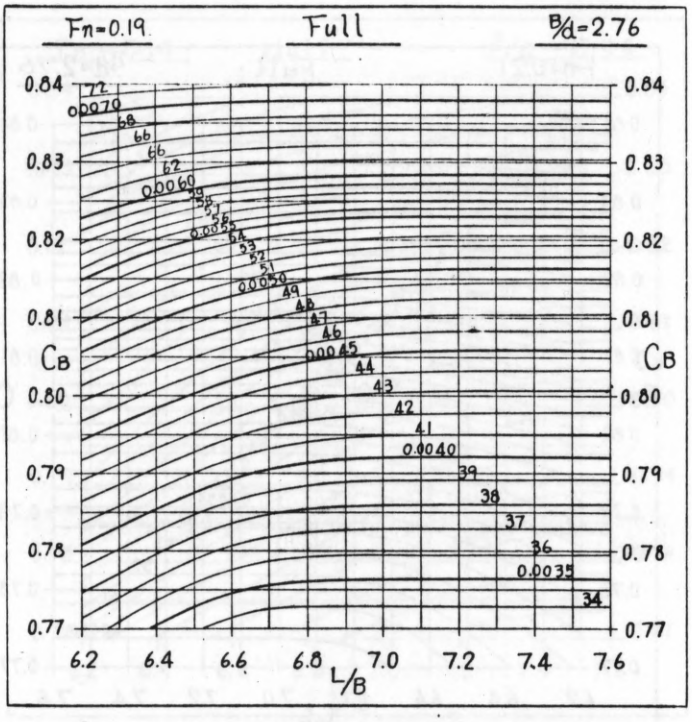

Fig.19 Contours of Residuary Resistance Coefficient

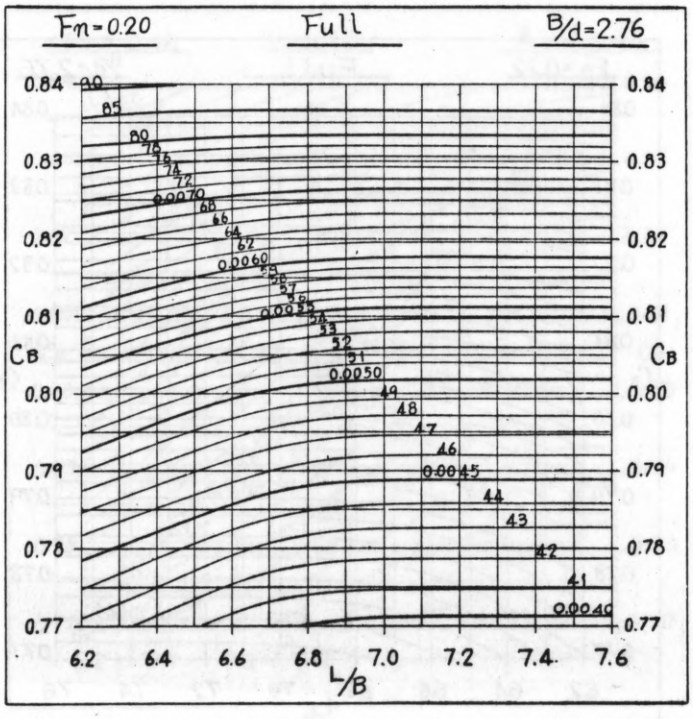

Fig.20 Contours of Residuary Resistance Coefficient

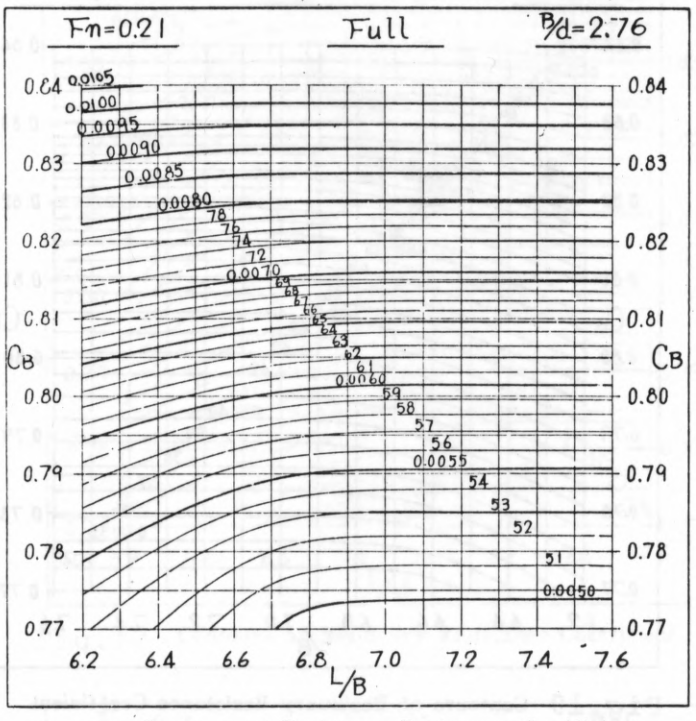

Fig.21 Contours of Residuary Resistance Coefficient

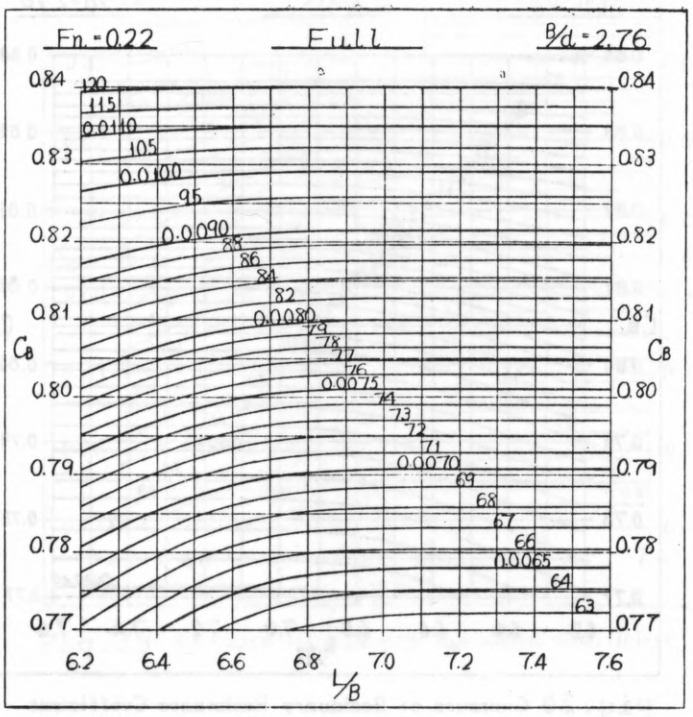

Fig.22 Contours of Residuary Resistance Coefficient

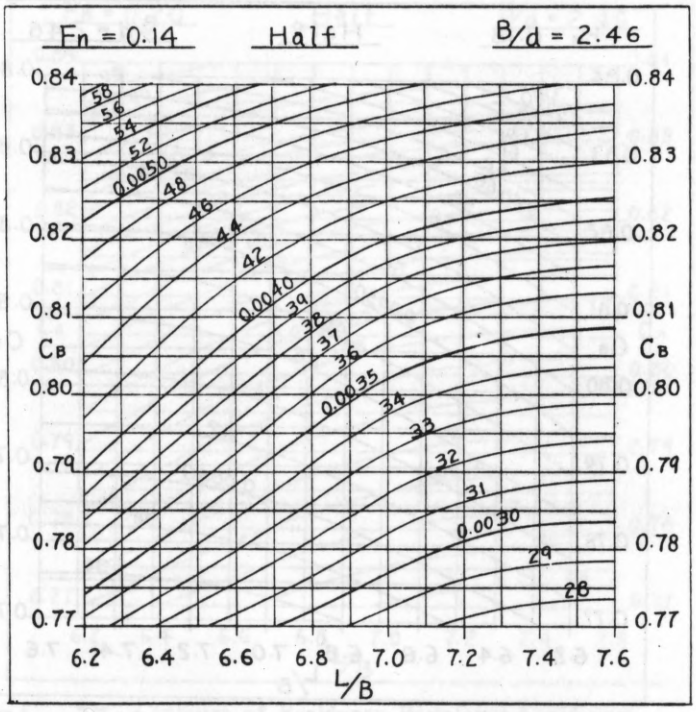

Fig. 23 Contours of Residuary Resistance Coefficient

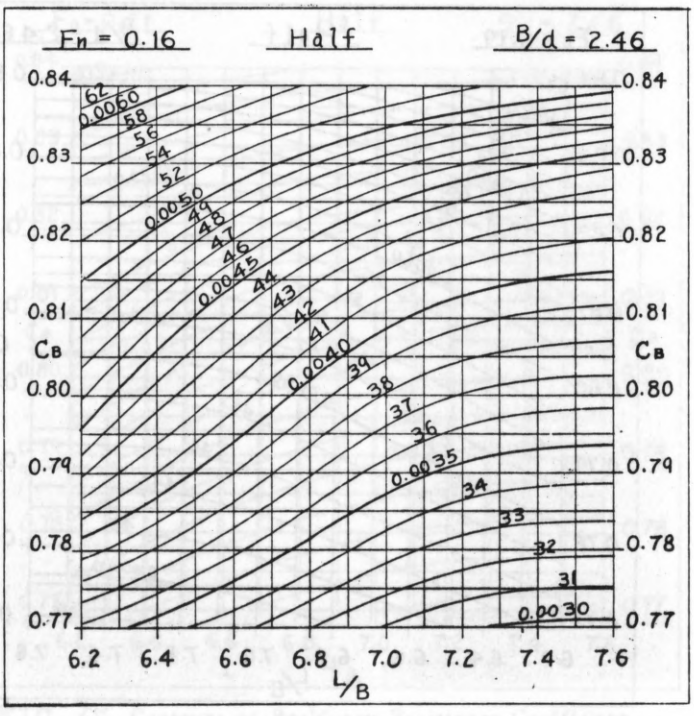

Fig. 24 Contours of Residuary Resistance Coefficient

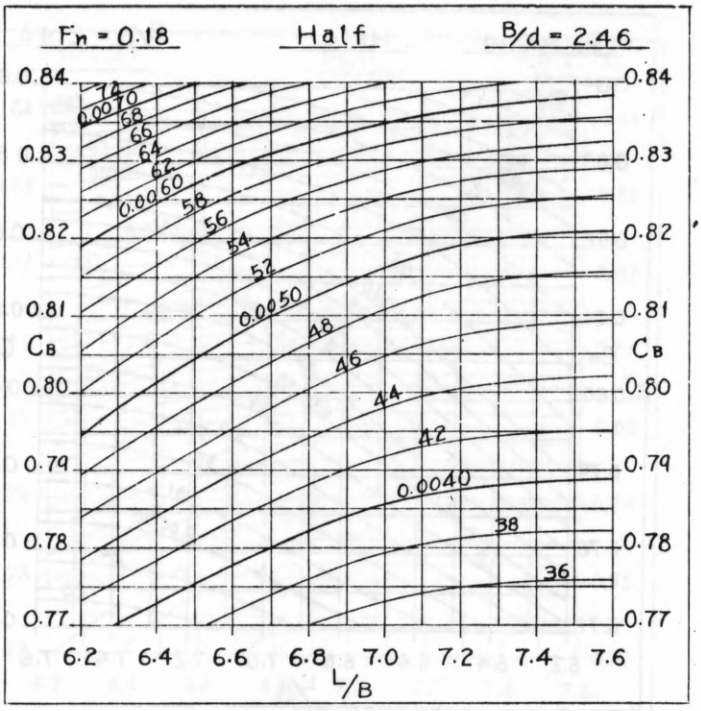

Fig. 25 Contours of Residuary Resistance Coefficient

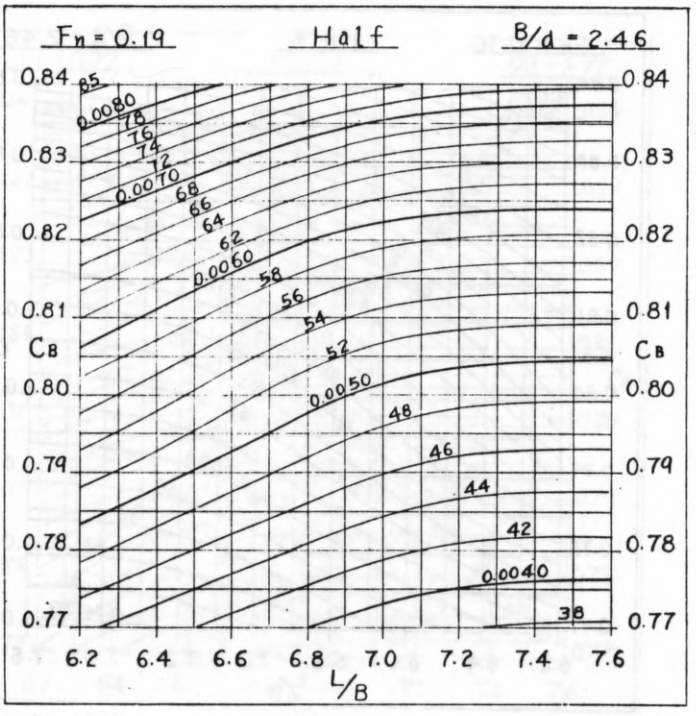

Fig. 26 Contours of Residuary Resistance Coefficient

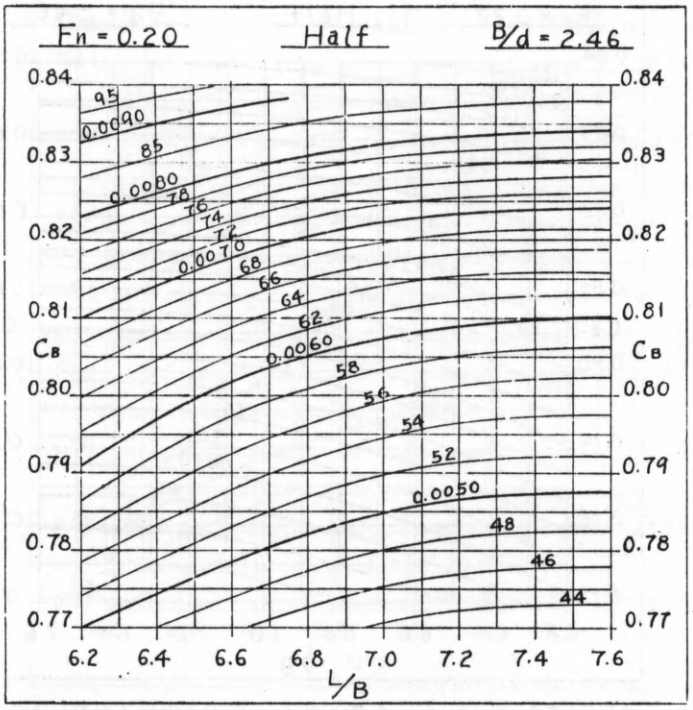

Fig.27 Contours of Residuary Resistance Coefficient

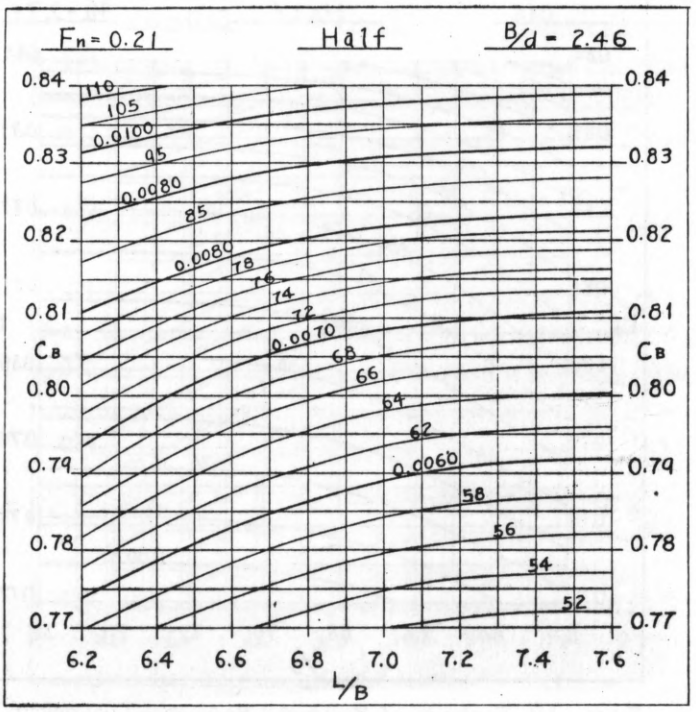

Fig.28 Contours of Residuary Resistance Coefficient

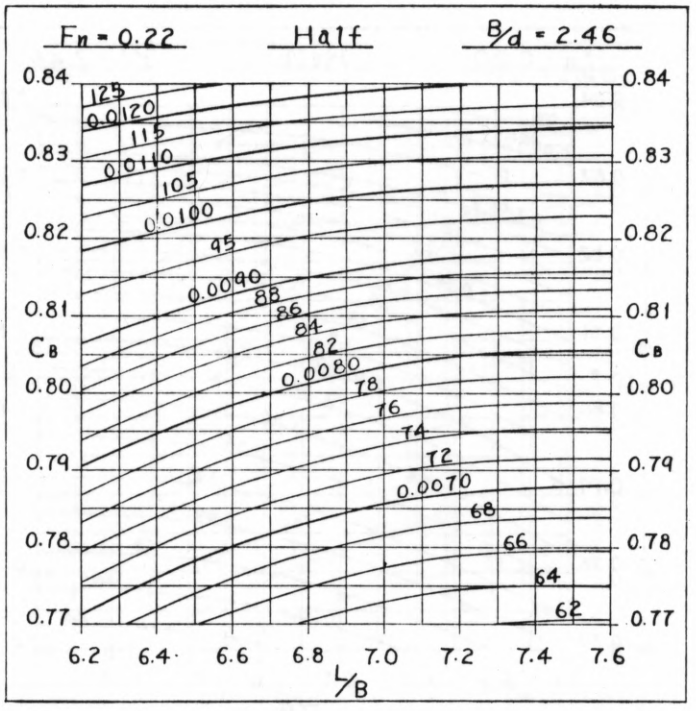

Fig. 29 Contours of Residuary Resistance Coefficient

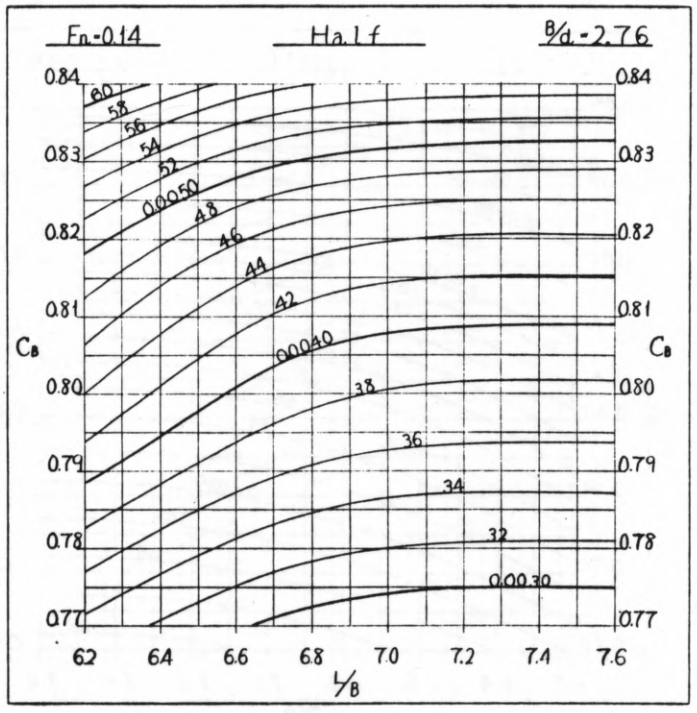

Fig. 30 Contours of Residuary Resistance Coefficient

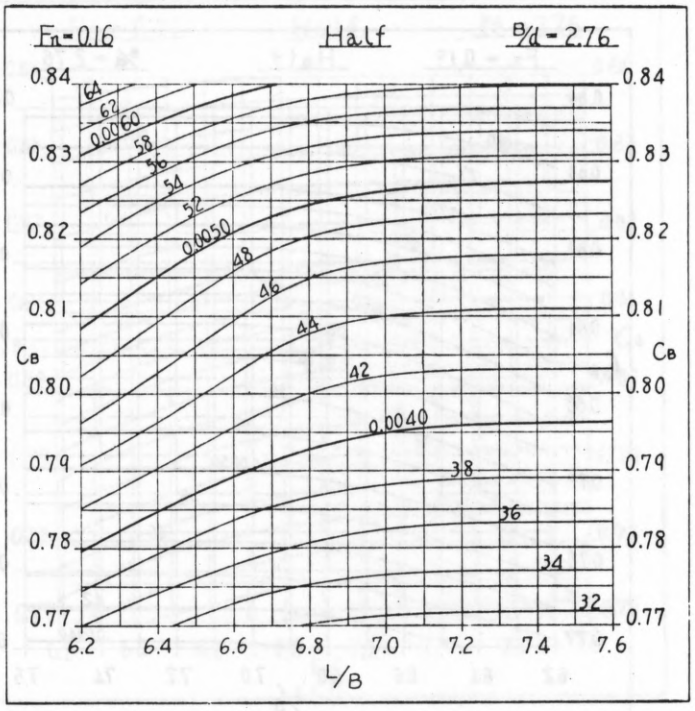

Fig.31 Contours of Residuary Resistance Coefficient

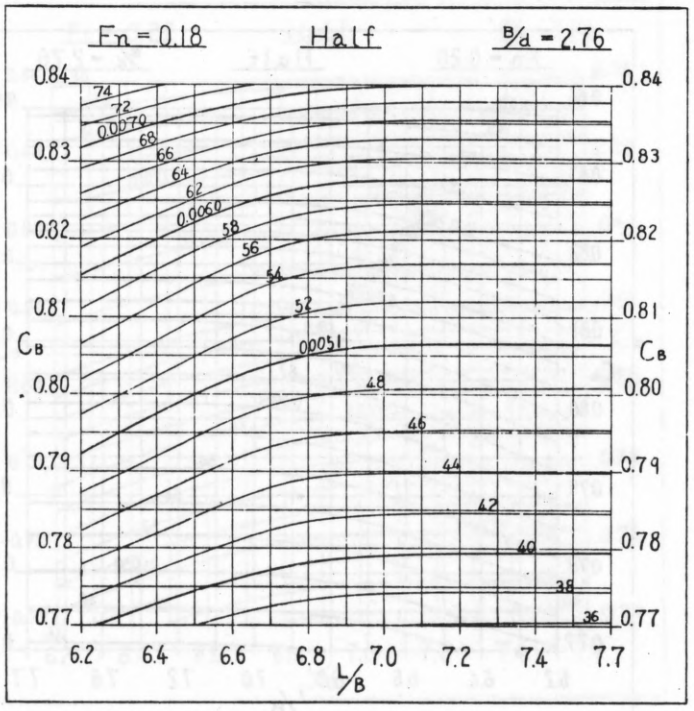

Fig.32 Contours of Residuary Resistance Coefficient

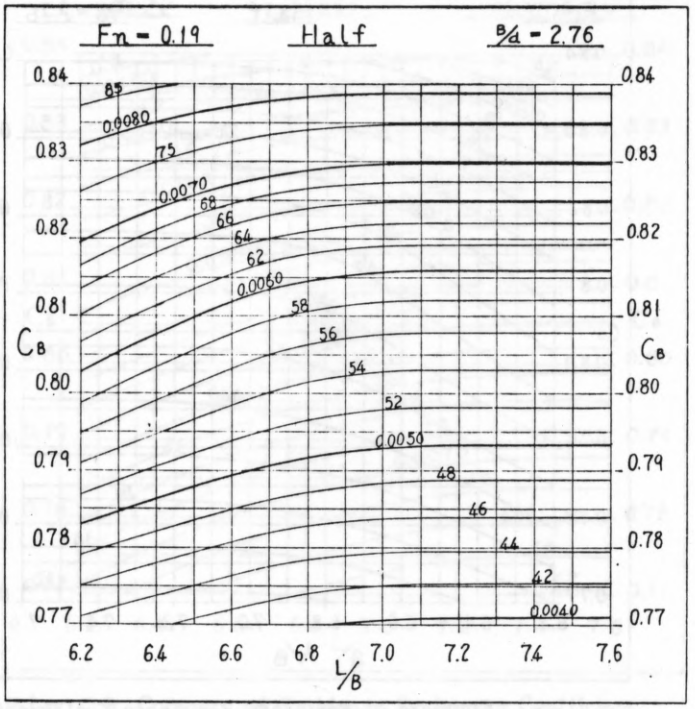

Fig.33 Contours of Residuary Resistance Coefficient

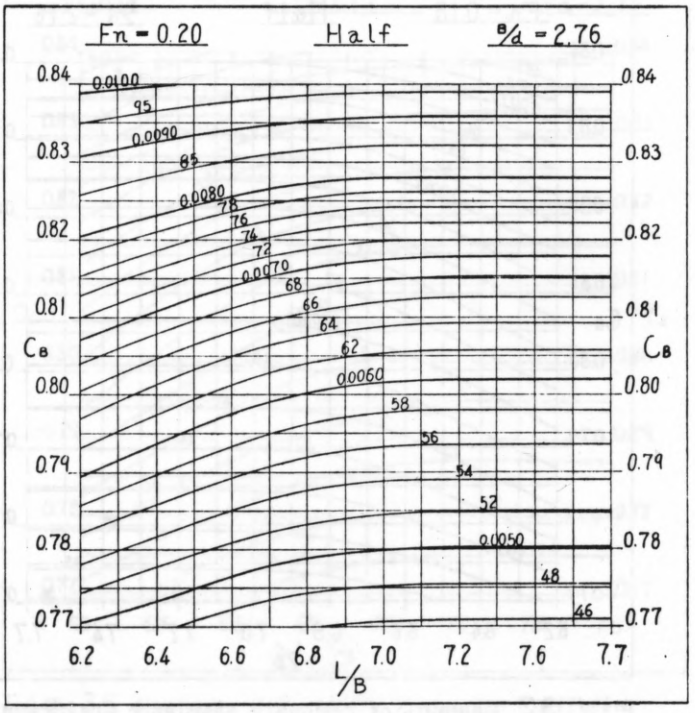

Fig.34 Contours of Residuary Resistance Coefficient

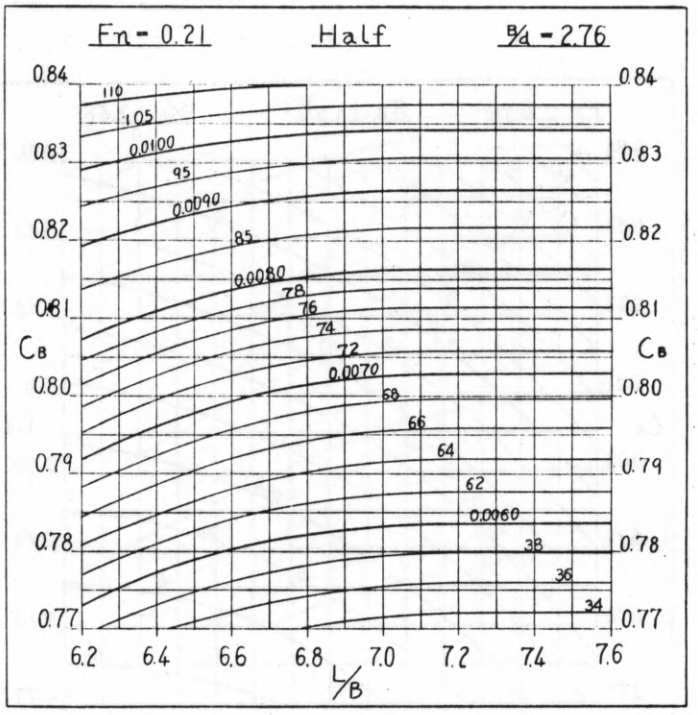

Fig.35 Contours of Residuary Resistance Coefficient

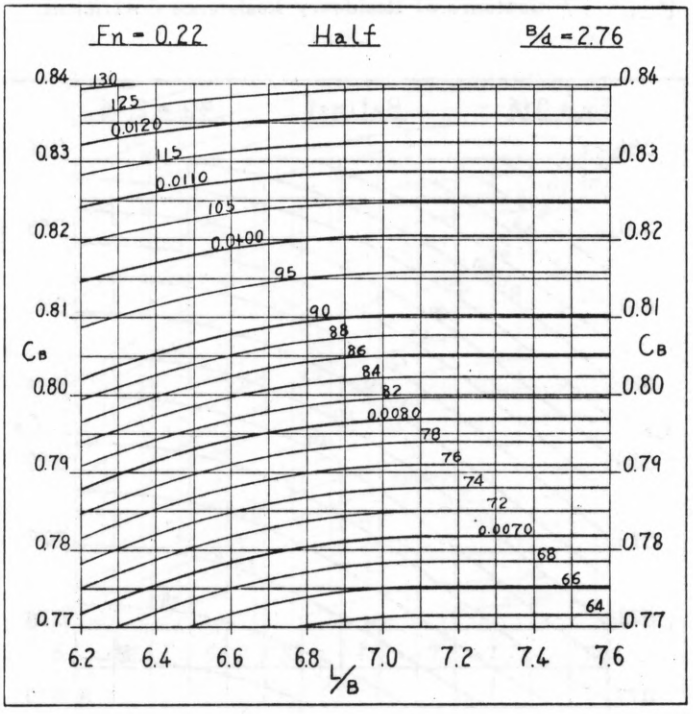

Fig.36 Contours of Residuary Resistance Coefficient

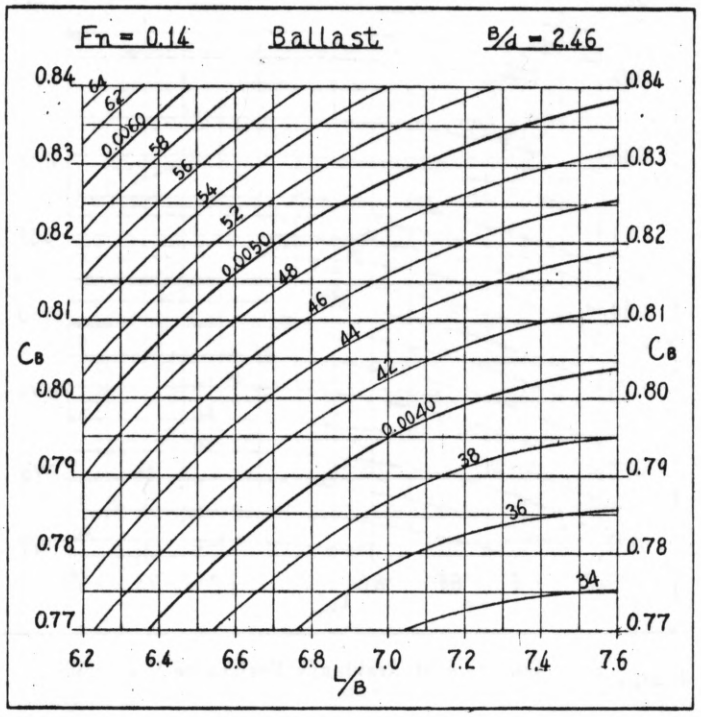

Fig. 37 **Contours of Residuary Resistance Coefficient**

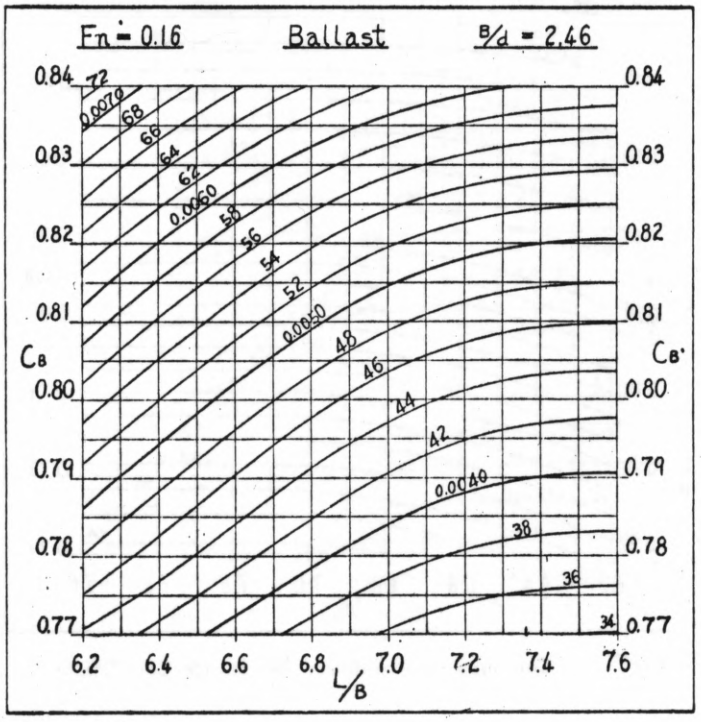

Fig. 38 **Contours of Residuary Resistance Coefficient**

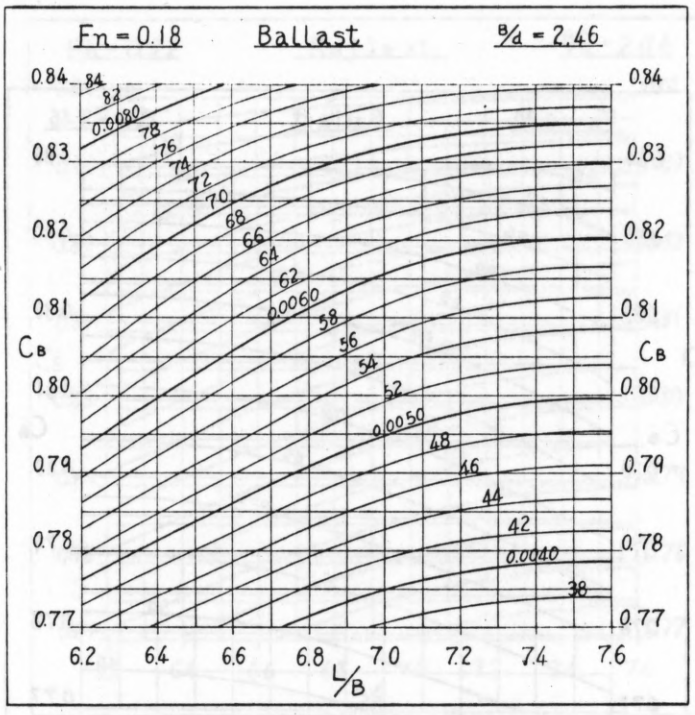

Fig. 39 Contours of Residuary Resistance Coefficient

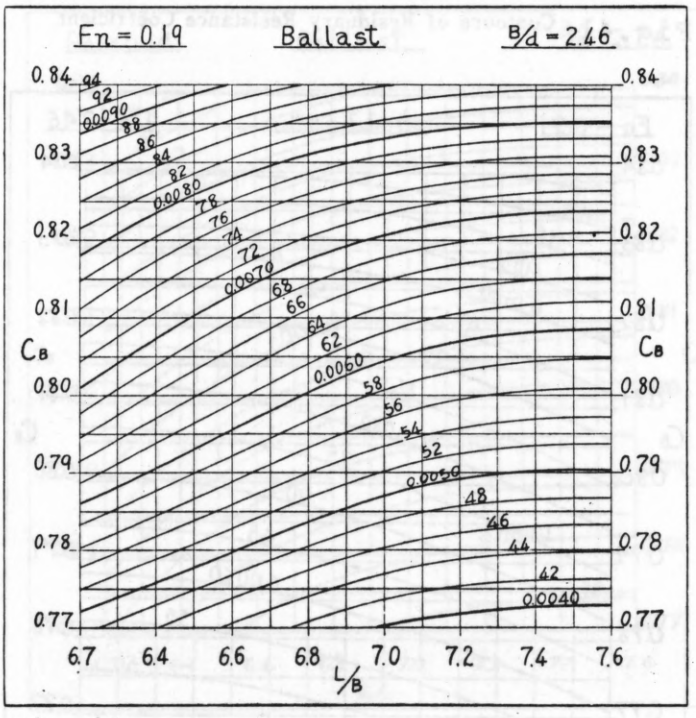

Fig. 40 Contours of Residuary Resistance Coefficient

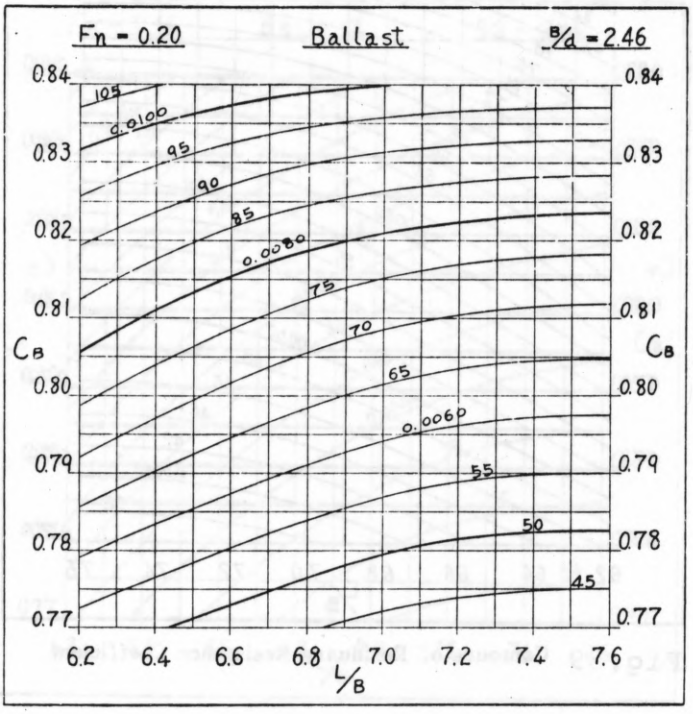

Fig.41 Contours of Residuary Resistance Coefficient

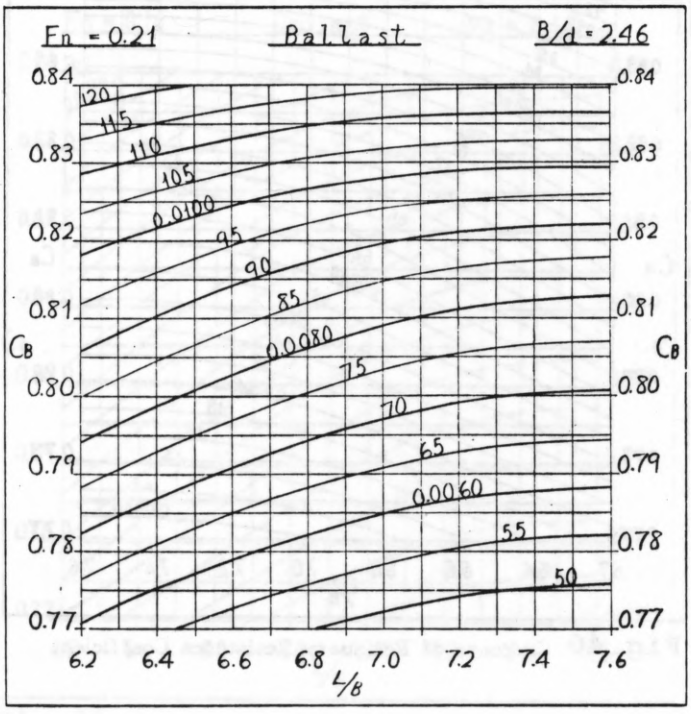

Fig.42 Contours of Residuary Resistance Coefficient

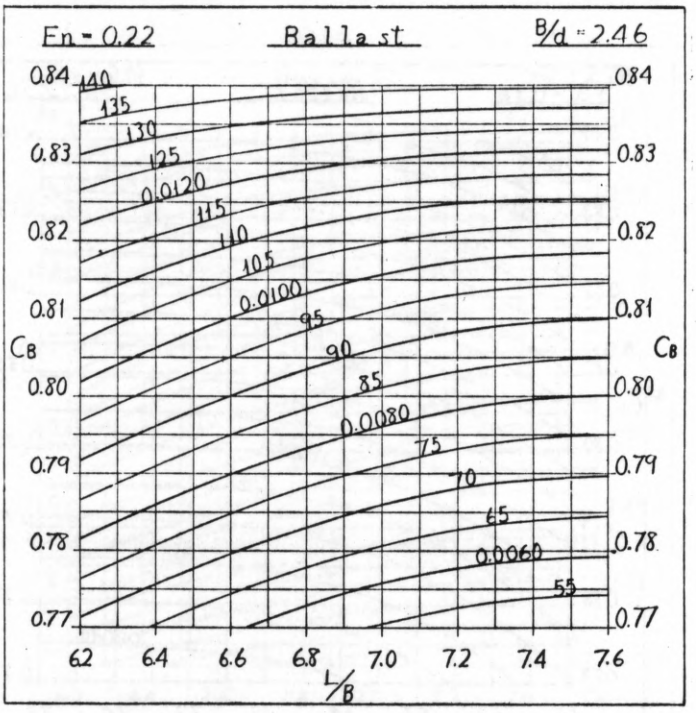

Fig.43 Contours of Residuary Resistance Coefficient

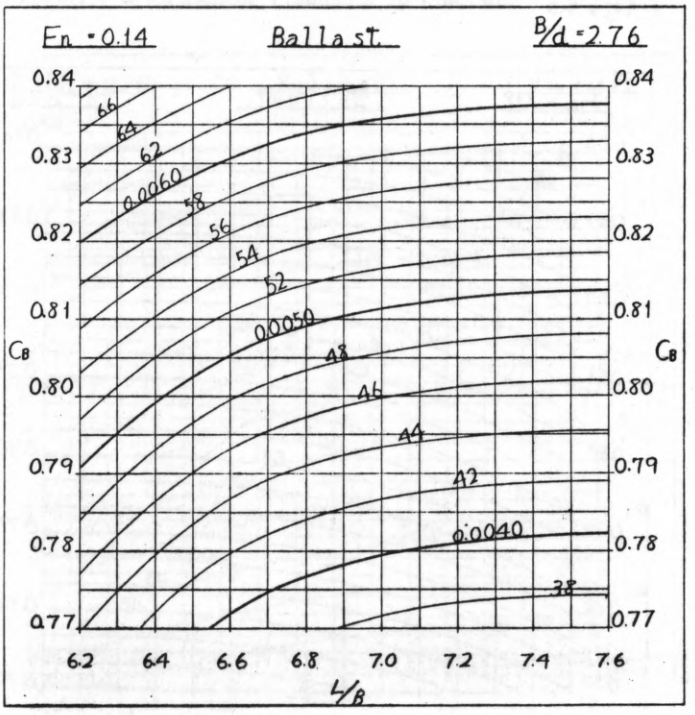

Fig.44 Contours of Residuary Resistance Coefficient

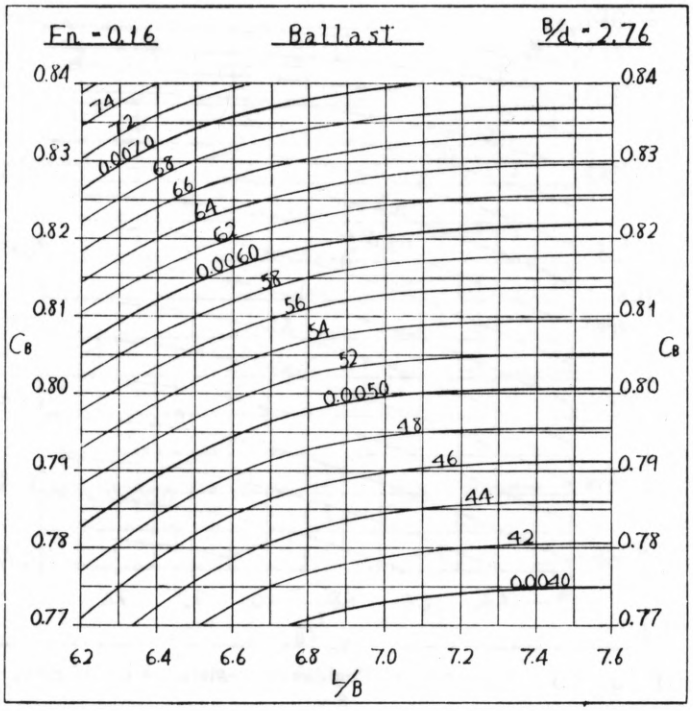

Fig.45 Contours of Residuary Resistance Coefficient

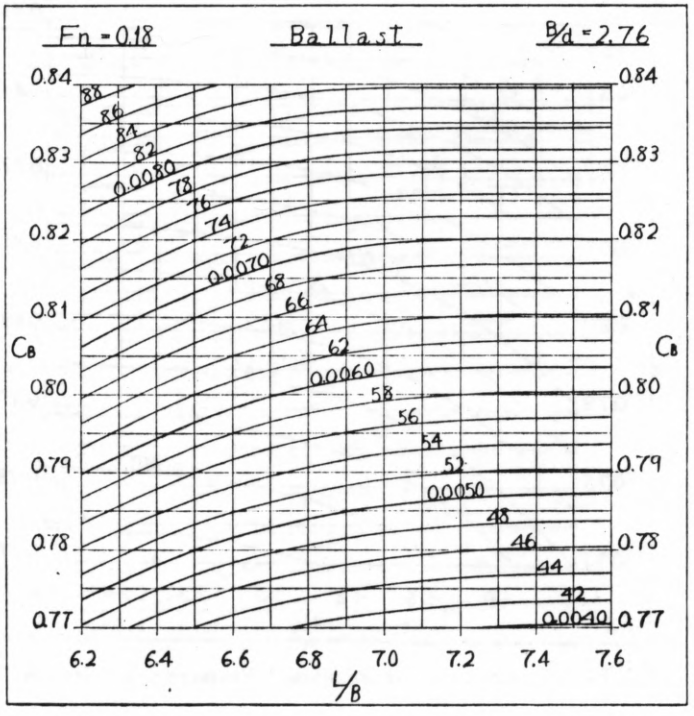

Fig.46 Contours of Residuary Resistance Coefficient

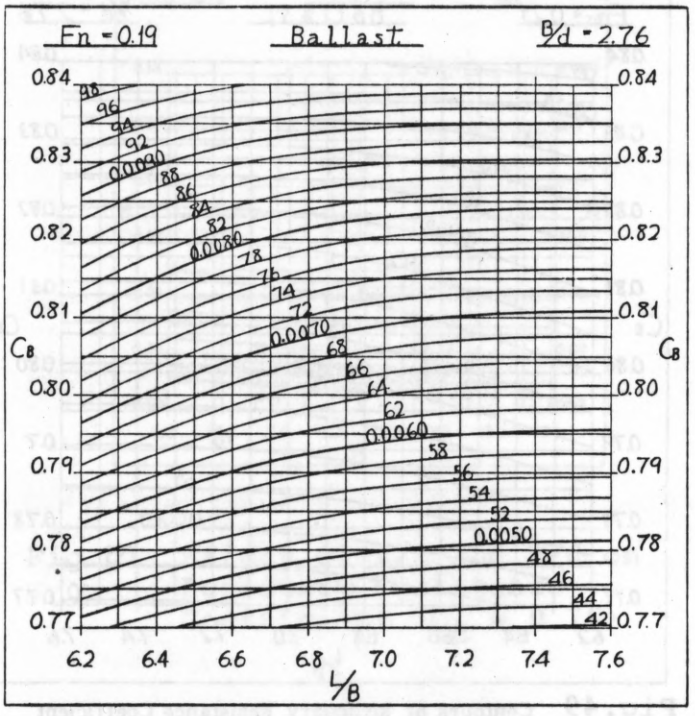

Fig.47 Contours of Residuary Resistance Coefficient

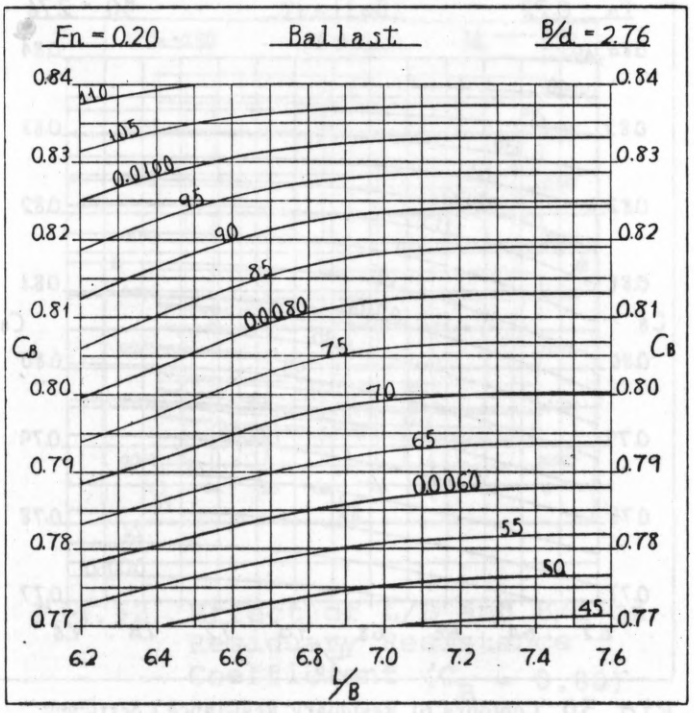

Fig.48 Contours of Residuary Resistance Coefficient

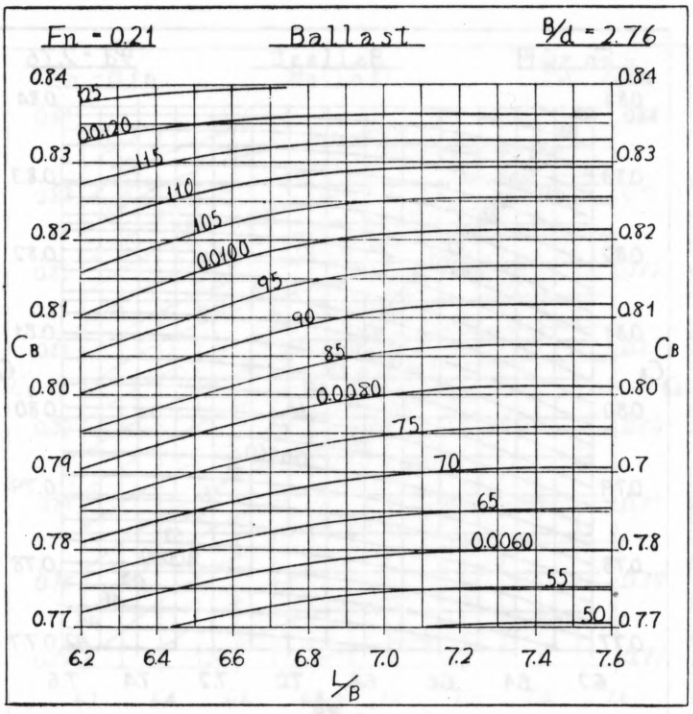

Fig.49 Contours of Residuary Resistance Coefficient

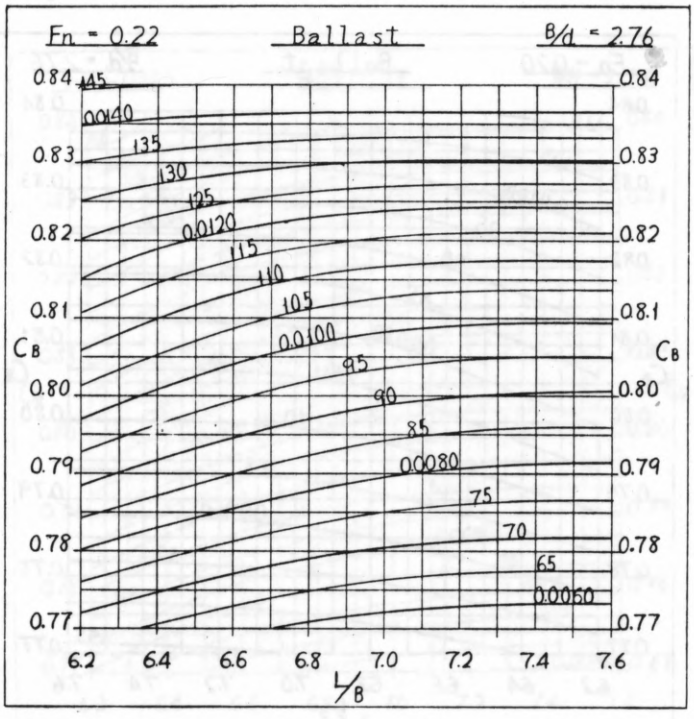

Fig.50 Contours of Residuary Resistance Coefficient

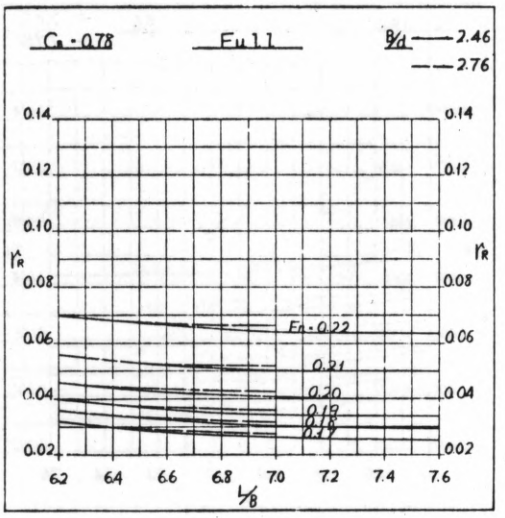

Fig.51 Effect of L/B and B/d on Residuary Resistance Coefficient (C_B = 0.78)

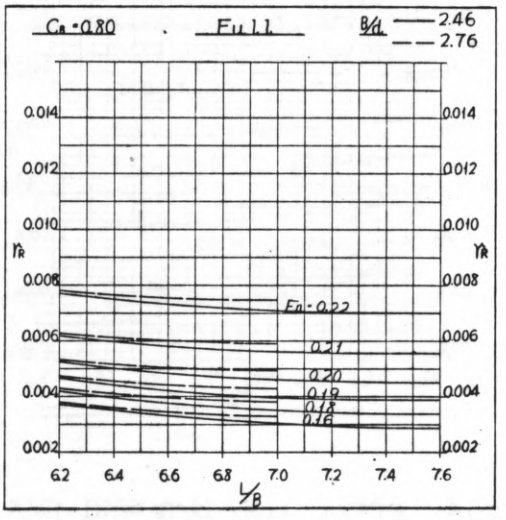

Fig.52 Effect of L/B and B/d on Residuary Resistance Coefficient (C_B = 0.80)

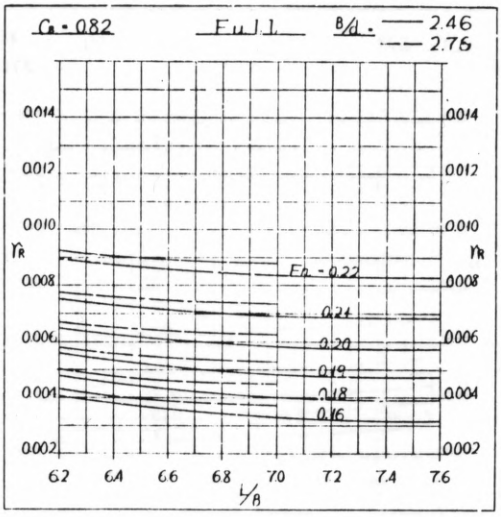

Fig.53 Effect of L/B and B/d on Residuary Resistance Coefficient (C_B = 0.82)

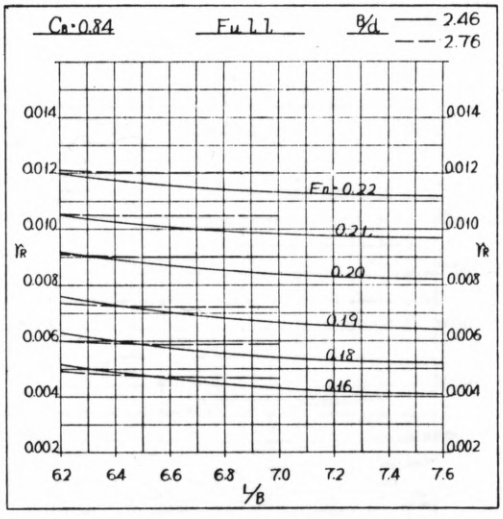

Fig.54 Effect of L/B and B/d on Residuary Resistance Coefficient (C_B = 0.84)

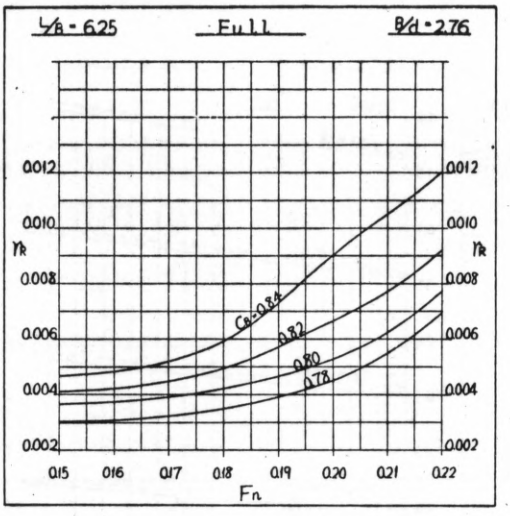

Fig.55 Effect of C_B on Residuary Resistance Coefficient

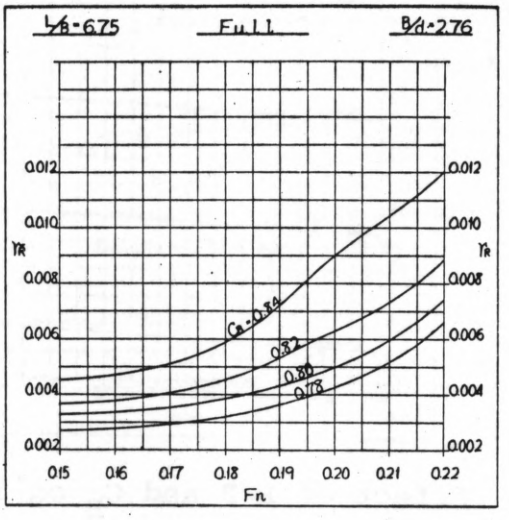

Fig.56 Effect of C_B on Residuary Resistance Coefficient

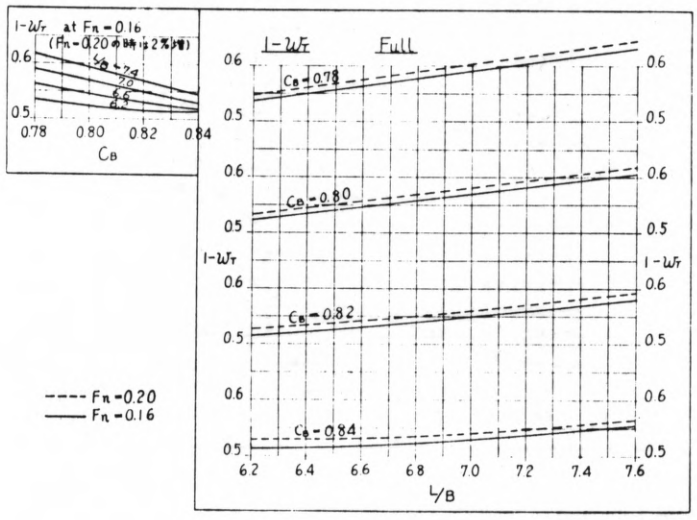

Fig.57 Effect of L/B and C_B on $1-w_T$

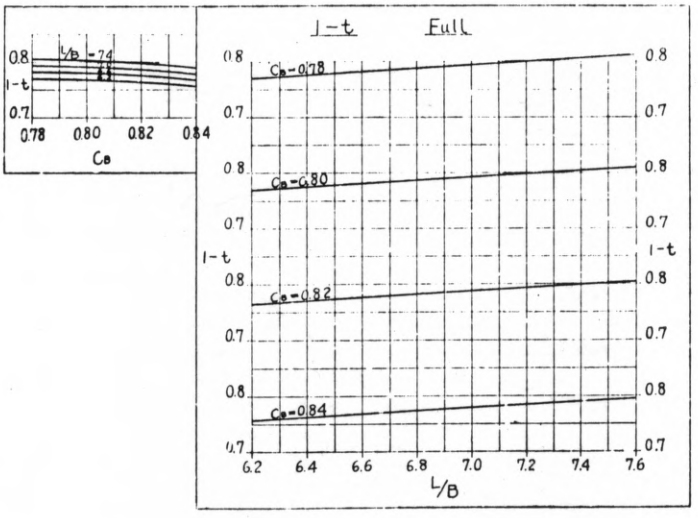

Fig.58 Effect of L/B and C_B on 1-t

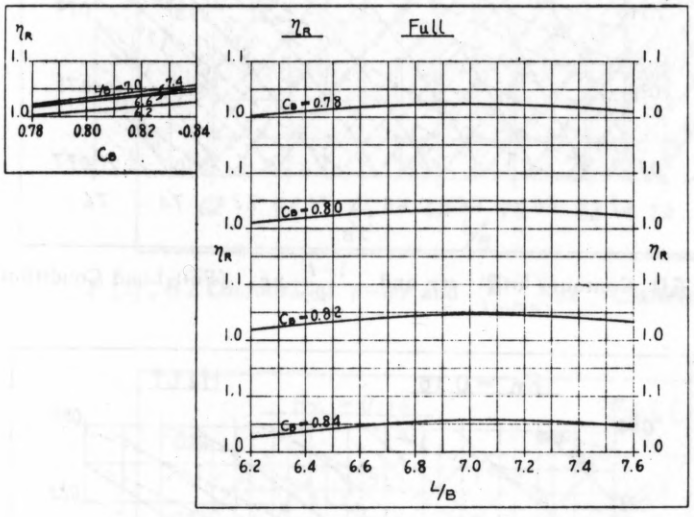

Effect of L/B and C_B on η_R

Fig. 59

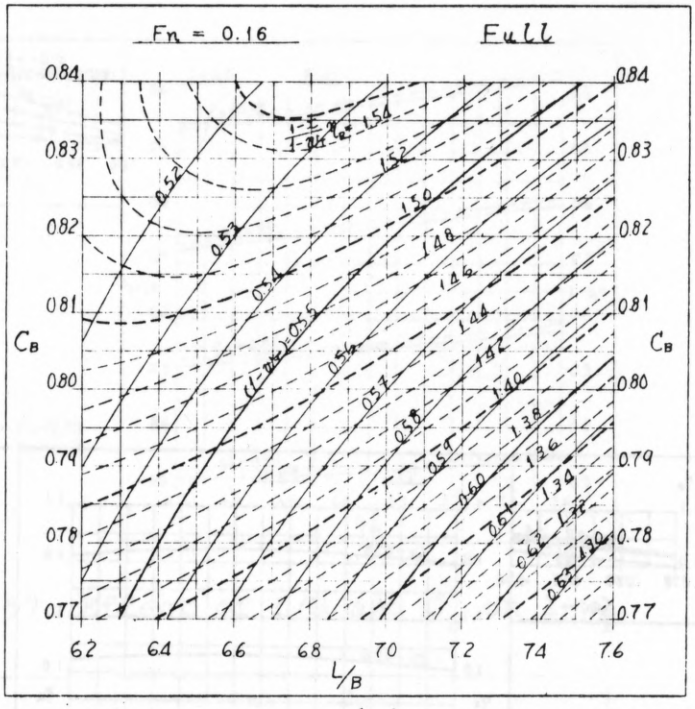

Fig.60 Contours of $1-w_T$ and $\frac{1-t}{1-w_T}\eta_R$ (Full Load Condition)

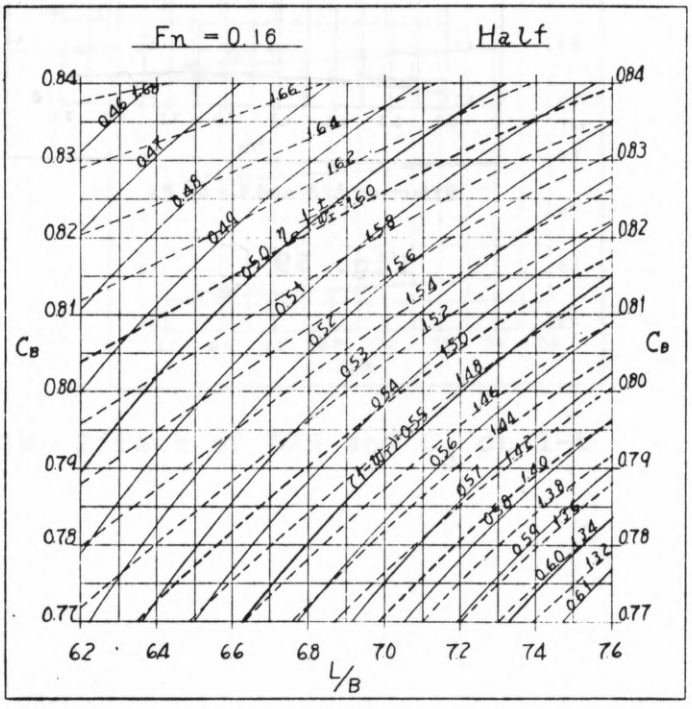

Fig.61 Contours of $1-w_T$ and $\frac{1-t}{1-w_T}\eta_R$ (Half Load Condition)

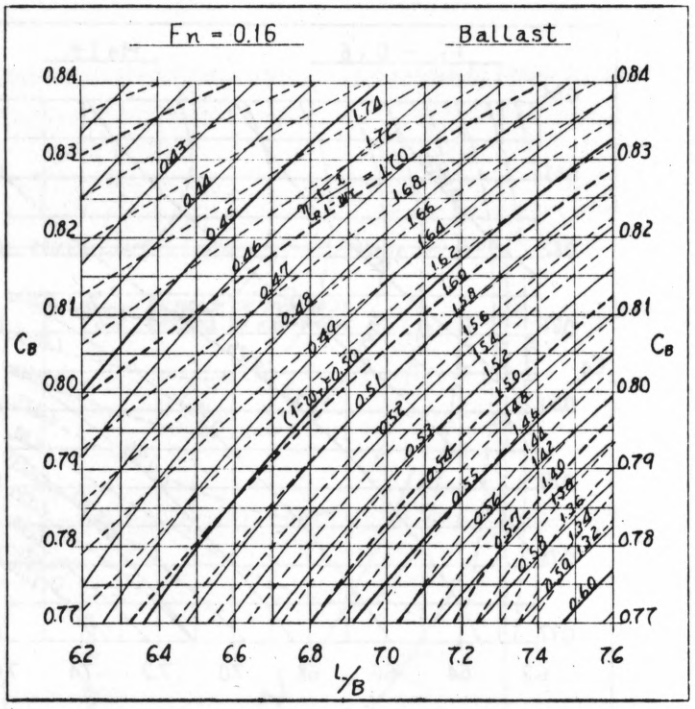

Fig. 62 Contours of $1-w_T$ and $\frac{1-t}{1-w_T}\eta_R$ (Ballast Condition)

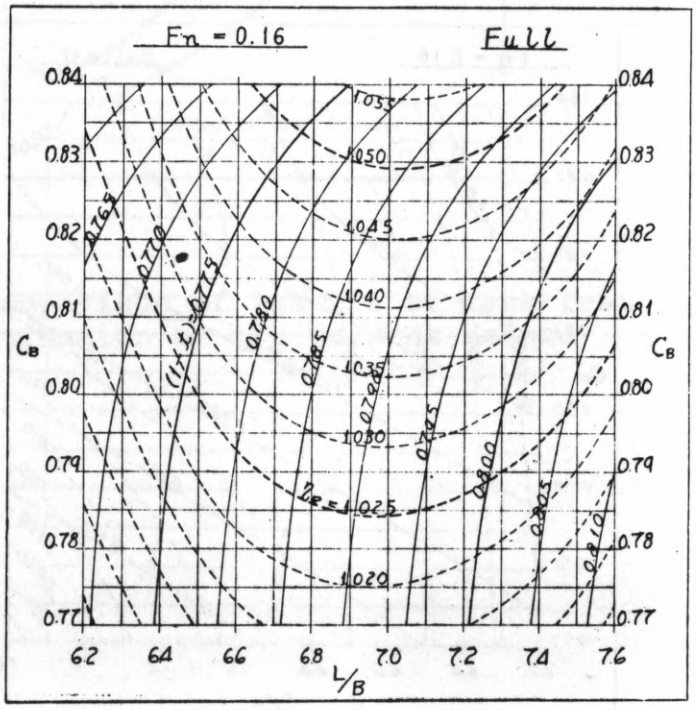

Fig. 63 Contours of $1-t$ and η_R (Full Load Condition)

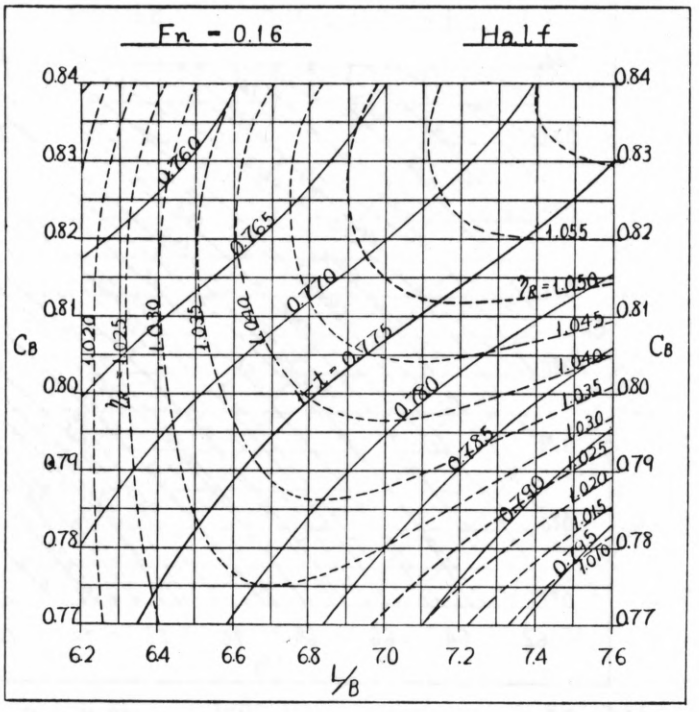

Fig.64 Contours of $1-t$ and η_R (Half Lead Condition)

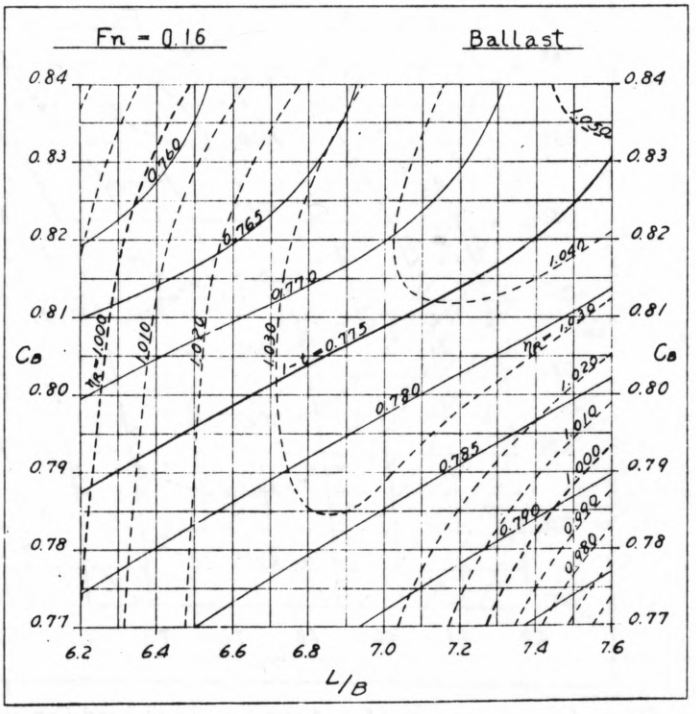

Fig.65 Contours of $1-t$ and η_R

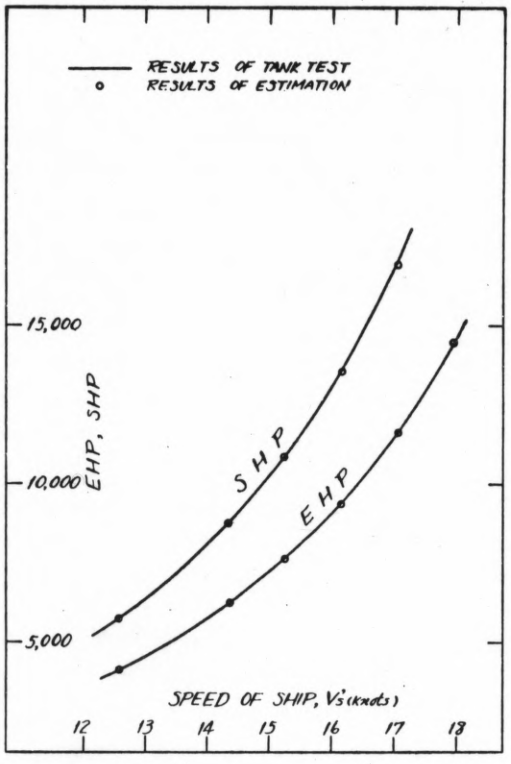

Fig.66 Comparison of Results of Tank Test and Estimation by the Present Method